Stiffness and grip force measurement using an eccentric mass motor: a dynamic model and experimental verification

Miquel Lopez

UNIVERSITY OF CALIFORNIA,
IRVINE

Stiffness and grip force measurement using an eccentric mass motor: a dynamic model and experimental verification

THESIS

in Mechanical and Aerospace Engineering

by

Miquel Batalle Lopez

2012

TABLE OF CONTENTS

List of figures iii
List of tables vii
Acknowledgments viii
Abstract of the thesis ix

List of figures

Figure 1: Schematic picture of a subject grasping an object. The eccentric mass motor, is placed on the outside of the finger, mounted onto a ring. 3

Figure 2: Schematic showing the mechanical model of our system (**Figure 1**). It is composed of four basic elements: eccentric mass dc motor, skin mechanical impedance, system mass and muscle stiffness which is in charge of increasing/decreasing the system stiffness (input).....7

Figure 3: State space representation suggests that we need to solve our two ODEs, found applying the Lagrange's method, for system acceleration and motor angular acceleration. Spaces 1x1 and 1x3 in matrix **Eq. 8** respectively.....9

Figure 4: Hill's muscle model considering three elements: Contractile component (CE), parallel elastic element (K_{PE}) and series elastic element (K_{SE}).....11

Figure 5: Graphical representation of the estimated stiffness and Normalized Force Level NFL, interpolated for the whole range of force. At the maximum force level 100%, we have a muscle stiffness of 816.1 N/m. Graph taken from [4], Fig. 4, subject B. 13

Figure 6: scheme showing skin mechanical impedance. Composed of a mass component (M), a damper component (C) and a spring component (K) which represents stiffness. All of them in parallel with each other.....15

Figure 7: Cantilever configuration of the finger. Where M_e is the mass of the dc motor, off-balance load and ring enclosure, and M_{Finger} is the finger mass. This model allows us to find the equivalent mass of the system M_1. 16

Figure 8: Regular pager dc motor by SolarBotics. It measures in at 7.05mm (0.277") diameter, 16.54mm (0.651") body length, and 21.7mm (0.854") overall length, with the shaft diameter of 1.01mm(0.039").....18

Figure 9: Picture showing SolidWorks assembly. Whole and partial views of the first setup. DC mass eccentric motor plus off-balance load which consists of three 2/56" screws and coupling. This assembly was designed to create a high vibratory effect to our system. 20

Figure 10: Picture showing SolidWorks assembly. Whole and partial views of the second setup. DC mass eccentric motor plus off-balance load which consists of one 2/56" screw and coupling. This assembly was designed to create a low vibratory effect to our system. 20

Figure 11: Motor velocity characteristic curve. Where the settling time is $\tau_s \approx 0.2$ s and motor velocity at equilibrium point 9553 R.P.M. 23

Figure 12: Torque and power characteristic curves, with a maximum torque of 0.1716 Nmm and a power peak at 43 mW. 24

Figure 13: Efficiency and Current characteristic curves, with efficiency peak at 52 % and with maximum current at 127 mA. 24

Figure 14: Cantilever beam setup. Eccentric mass dc motor is standstill. The beam was slid in and out in order to change the stiffness and measure the vibration and speed of the dc motor. 31

Figure 15: Picture of the whole cantilever beam setup. On the right, beam anchored to the table, eccentric mass dc motor rotating. In the middle, national instrument, stroboscope and power supply. On the left side of the picture, computer with Matlab acceleration data plots. 32

Figure 16: Cantilever beam model. 33

Figure 17: Impulse response for a span of 119.4 mm or 1500 N/m. 34

Figure 18: Impulse response fit curve for stiffness 1500 N/m. Both curves overlap, meaning that the fit is good. 35

Figure 19: Damping ratio evolution for thirteen levels of stiffness considered. In N/m: 250, 500, 625, 750, 1000, 1500, 3000, 4500, 6000, 7500, 9000, 10,500 and 12,000 36

Figure 20: Picture of the non- interposed ring sensor setup. The subject is wearing the device on the intermediate phalange of the index finger 37

Figure 21: Picture showing ring sensor experiment setup. On the right, force transducer handgrip plus ring sensor worn by the subject. In the middle national instrument to acquire data. On the left side, power supply. 39

Figure 22: Experiment #1. Plot showing the comparison between simulation and data recorded by the accelerometer and stroboscope for stiffness levels [N/m]: 250, 500, 625, 750, 1000, 1500, 3000, 4500, 6000, 7500, 9000, 10,000 and 12,000 50

Figure 23: Experiment #1. Plot showing the evolution of motor velocity over time for the simulation. 50

Figure 24: Experiment #1. Plot showing the resonance analysis for experiment #1. Simulation vs. Experiment results. 51

Figure 25: Experiment #1. Plots of vibration displacement for every stiffness, max amplitude at steady state taken in order to build **Figure 24**. 52

Figure 26: Experiment #1. Plot showing the natural frequency of the system for each stiffness vs. the motor velocity. When they match up the system is resonating. 53

Figure 27: Experiment #1. Plot showing the vibration acceleration as a function of stiffness. System resonating for a stiffness of 1500 N/m. 53

Figure 28: Experiment #1. Acceleration profile for every stiffness in g-force (9.81 m/s^2). Data used to build **Figure 27**. Plot for K = 1500 N/m, the accelerometer was saturated (acceleration > 6G) since the system is resonating. 55

Figure 29: Experiment #**2**. Plot showing the comparison between simulation and data recorded by the accelerometer and stroboscope for stiffness levels [N/m]: 250, 500, 625, 750, 1000, 1500, 3000, 4500, 6000, 7500, 9000, 10,000 and 12,000 56

Figure 30: Experiment #**2**. Plot showing the evolution of motor velocity over time for the simulation. 57

Figure 31: Experiment #**2**. Plot showing the natural frequency of the system for each stiffness vs. the motor velocity. When they match up the system is called to be in resonance. 57

Figure 32: Experiment #**3**. Plot showing the comparison between simulation and data recorded by the accelerometer and stroboscope for stiffness levels [N/m]:

250, 500, 625, 750, 1000, 1500, 3000, 4500, 6000, 7500, 9000, 10,000 and 12,000.....58

Figure 33: Experiment #**3**. Plot showing the evolution of motor velocity over time for the simulation.....58

Figure 34: Experiment #**3**. Plot showing the natural frequency of the system for each stiffness vs. the motor velocity. When they match up the system is called to be in resonance.....59

Figure 35: Plot showing the voltage analysis of sensitivity.....60

Figure 36: Plot showing the off-balance load analysis of sensitivity.....61

Figure 37: Plot showing the system mass analysis of sensitivity.....62

Figure 38: Plot showing the evolution of motor velocity as we vary the voltage for constant levels of stiffness.....63

Figure 39: Experiment #1. Force transducer grip force measurements and accelerometer data profile.....66

Figure 40: Experiment #1. Normalized force level versus motor frequency. Data from **Figure 39**.....67

Figure 41: Experiment #1. Comparison between simulation and experiment. Muscle stiffness is related to NFL (%) through **Figure 5**.....68

Figure 42: Experiment #2. Force transducer grip force measurements and accelerometer data profile.....69

Figure 43: Experiment #2. Normalized force level versus motor frequency. Data from **Figure 42**.....69

Figure 44: Experiment #2. Comparison between simulation and experiment. Muscle stiffness is related to NFL (%) through **Figure 5**.....70

Figure 45: Plot showing the trade-off between ring sensor sensitivity and g-force, and the optimal point in red.....72

Figure 46: Optimal set of parameters, red point.....73

Figure 47: Optimal system behavior.....74

List of tables

Table 1: Masses in our system, with **Eq. 11** and **Eq. 12** it gives us a total mass of ≈ 16 g. 17

Table 2: Regular pager dc motor characteristics. 1.5V gives 17.5mA free draw current (120mA stall) at 9700RPM. 3V gives 22mA free (260mA stall) at 18,420RPM. 5V operation give 32.1mA free (420 stall) at 31,900RPM. 18

Table 3: Values of off-balance load and eccentricity for sets one and two. 20

Table 4: DC Motor variables calculated using **Table 2**, **Eq**. **14** and **15**. Motor winding resistance measured using a multimeter, and for the motor moment of inertia we picked a low value since it is very insignificant compared to the off-balance load mounted onto the shaft.....22

Table 5: DC Motor simulation parameters for V = 1.5 volts. 23

Table 6: Beam total mass for each stiffness level. 34

Table 7: Parameters bounds and number of steps taken, which also define the increment size. . 47

Table 8: Optimal parameters. 71

Acknowledgments

I would like to thank my advisor for welcoming me in the Biomechatronics lab, for his great advise and motivation, and giving me the opportunity of living such an incredible experience because I have truly learnt a lot.

Thank you to the members of the Biomechatronics lab, for helping me with my experiments and throughout the whole year. Thanks to the rest of the committee members, Professor James Bobrow and Professor Mark Bachman.

Additionally, my sincere appreciation to the Balsells Fellowship Program for offering me the opportunity of pursuing my Master's in Mechanical and Aerospace Engineering at the University of California, Irvine. Specially thanks to Professor Roger Rangel for his support.

Finally, special thanks to all my family for their support.

Abstract of the thesis

Stiffness and grip force measurement using an eccentric mass motor: a dynamic model and experimental verification

by

Miquel Batalle Lopez
Master of Science in Mechanical and Aerospace Engineering
University of California, Irvine, 2012

Loading can dramatically reduce the vibratory displacement and the operating frequency in vibrotactile systems implementations that use an eccentric mass motor, but this phenomenon is not well modeled or understood. In this work, we derive a dynamic model of this phenomenon and implement a system for measuring stiffness and grip force that take advantage of this phenomenon. The system is based on a non-interposed sensing approach using an eccentric mass dc motor mounted on the outside of the index finger. If the device were to be worn as a wearable sensor, it could be embedded in a ring. The basic idea is that a person could wear the ring sensor and through it measure the stiffness and grip force when squeezing various objects, without requiring the ring sensor to actually contact the object. The results show that grip force and muscle stiffness vary with motor velocity (operating frequency) and thus that the measurement

of velocity can be used to infer grip force and stiffness. With the validated model, we also developed an optimization routine which computes the best design parameters for inertial load and voltage to maximize the phenomenon. This provided insight into the optimal parameters that should be used in an actual ring sensor design to achieve high performance by attaining a good trade-off between high sensor sensitivity and low level of vibration.

1 Introduction

Eccentric mass motors are used in a wide range of applications, including vibration alerting functions in cell phones and pagers, and vibrotactile systems for providing haptic feedback. Vibrotactile systems take advantage of the body's sense of touch for the conveyance of information, hence the device, i.e. the eccentric mass motor, is usually enclosed within a housing and mounted to the skin. Human skin impedance is composed of three components: mass, a springy component and a viscously damping one. It is also known that the human skin is highly non-linear [3] and that its impedance varies with frequency and location on the body, as well as the loading applied to it [1],[2]. Hence, depending on the design of a vibrotactile system device, loading can dramatically reduce the vibratory displacement and the operating frequency [1]. This phenomenon is disadvantageous for these systems since they should ideally produce a displacement output that is relatively independent of loading to generate a consistent sensation for the user. Developers of vibrotactile systems have suggested that in order to avoid these adverse effects the mechanical properties of the skin should carefully be taken into consideration in device design [2]. Yet, to our knowledge, there are no dynamic models of the interactions of eccentric mass motors and human skin that could be used to guide device design. In the work presented here, we present such a dynamic model and verify it experimentally.

We also show using the model and several experiments how the loading phenomenon can be used to our advantage in order to measure hand stiffness and grip force without interposing the sensor between the hand and the object gripped.

Vibration has previously been taken advantage of in order to measure the impedance of the human hand or arm, however never grip force to our knowledge, and not in a non-interposed way. For instance, a vibratory device for measuring the arm's geometrical mechanical impedance was developed [7]. This device is larger than the ones used in vibrotactile systems, being about the size and shape of a coffee mug. Essentially, the human hand that holds the device receives a dynamic force exerted by the centrifugal force due to the rotating mass. Ultimately, acceleration signals caused by the vibration are correlated with the perturbing force in order to obtain hand mechanical impedance.

In our case, we are interested in the measurement and estimation of the human hand's stiffness during gripping, which is also an active research topic. For example, for this application, a grasp perturbator to measure finger stiffness during pinch grip operations was recently developed [4]. It relies on a simple idea: the device displaces the relative position of thumb and index fingers by a known distance and measures the reaction force exerted by the fingers. The device also shows a linear relationship between finger stiffness and grip force. A disadvantage of this device is that it must be interposed between the fingers to measure stiffness. That is, it can only be used to measure hand stiffness when the hand is gripping the experimental apparatus itself. In this project, we show how it is possible to take advantage of the loading effects of vibratory systems in order to create a non-interposed grip force sensor.

2 Materials and Methods

2.1 Basic Phenomenon and Overview of Methods

In this section a dynamic model for a system for measuring stiffness and grip force is presented. It is based on a non-interposed sensing approach using an eccentric mass dc motor mounted on the outside of the index finger, between the distal interphalangeal and proximal interphalangeal joints (**Figure 1**). If the device were to be worn as a wearable sensor, it could be embedded in a ring. The basic idea is that a person could wear the ring sensor and through it measure the stiffness and grip force when squeezing various objects, without requiring the ring sensor to actually contact the object.

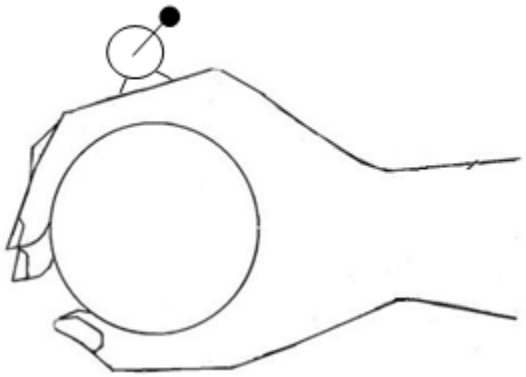

Figure 1: Schematic picture of a subject grasping an object. The eccentric mass motor, is placed on the outside of the finger, mounted onto a ring.

The basic phenomenon used to measure stiffness and grip force is as follows. The off-balance load carried by the dc motor causes the finger to vibrate. For a lower impedance system the vibratory displacement is high, creating a greater inertial load on the motor. Since the motor is driven at a constant voltage, the dc motor spins at lower velocities. Higher impedances cause the motor to speed up. Because the impedance of the finger and the grip force are directly related, a lower force generates a high vibratory displacement, and thus low velocities for the motor. On the other hand, high grip forces cause the motor to speed up.

To study this phenomenon we carried out two experiments:

- Cantilever beam with variable length: The goal of this experiment is to quantify the relationship between motor velocity and stiffness in a controlled setting. Changing the length of the beam, we varied the stiffness of the system, and as a result the motor (mounted at the end of the beam) changed its velocity as well. This experiment allowed us to investigate the sensitivity of each parameter in our model (**Figure 2**).
- Ring Sensor: The purpose of this experiment was to take advantage of the phenomenon to build a non-interposed grip force sensor. We built a simple ring and tested it in order to demonstrate how we can measure grip force and muscle stiffness by correlating them with motor velocity.

We derived the equations of motion applicable to both experiments and simulated them using Matlab. This procedure validated the mathematical model and confirmed our hypothesis that grip force and muscle stiffness vary with motor velocity.

With the validated model, we developed an optimization routine which computes the best design parameters for inertial load and voltage to maximize the phenomenon. This provided insight into the optimal parameters that should be used in an actual ring sensor design to achieve high performance by attaining a good trade-off between high sensor sensitivity and low level of vibration.

The basic idea is that, designing a grip force sensor using an eccentric mass dc motor, we want it to be able to increase/decrease its angular velocity very rapidly and as much as possible when there is a change in muscle stiffness/grip force. However, we do not want the device to be annoying for the wearer, so it needs to work at the lowest level of vibration possible.

The dependence of the system to parameters such as voltage, total mass and off-balance load is also studied through simulations. Quantifying how sensitive the system is to a change in these parameters provides insight into the phenomenon. In other words, we quantified what happens when we raise and drop the voltage, when we mount a light or a big off-balance load or, how our system is going to behave if instead of using a light housing for our dc motor we use a heavy one.

2.2 Mathematical Model

The mathematical model can be divided into four parts: skin mechanical impedance, muscle stiffness, system total mass and eccentric mass dc motor (**Figure 2**).

The basic idea is that an increase in grip force is associated with an increase in muscle stiffness, as muscle become stiffer as they contract. The skin is compressed also during grip and it also increases its impedance. As a result of this action, the dc motor velocity changes. The model results in a second order system, where skin and muscle stiffnesses are in parallel, which means that the total stiffness is the sum of one plus the other. Skin damping remains in parallel with total stiffness and skin mass can be added to the total mass.

In **Figure 2**, the dc motor is modeled by θ, τ and J which respectively are motor angular position, torque and moment of inertia. M_1 accounts for the mass of our system (off-balance load, dc motor, ring and finger mass). The constant m is the mass of the off-balance load and l is its eccentricity. Skin mechanical impedance is represented by M_2, C and K_{Skin} which respectively are mass, damping and stiffness of the area of skin affected by the vibration. For the muscle, we used a simplified version of the hill's model. Hence K_{Muscle} is its stiffness. X is the system amplitude of vibration or vibratory displacement. Finally, for our calculations we consider only one total mass M which is the sum of M_1 and M_2.

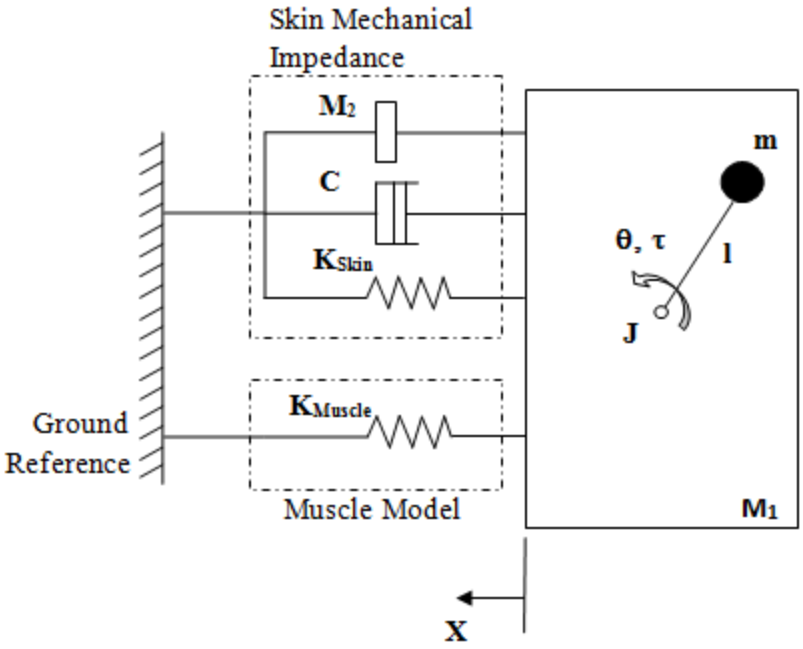

Figure 2: Schematic showing the mechanical model of our system (**Figure 1**). It is composed of four basic elements: eccentric mass dc motor, skin mechanical impedance, system mass and muscle stiffness which is in charge of increasing/decreasing the system stiffness (input).

The dynamic equations of our system are obtained using Lagrange's Method. The basic idea is to calculate kinetic energy (**Eq. 2**), potential energy **(Eq. 5**) and dissipative energy (**Eq. 6**) for the system as a function of every DoF (degree of freedom). Then, applying the Lagrangian (**Eq. 1**) and identifying all the existing forces and torques, we can obtain the differential dynamic equations. We have a two DoF system, where the variables are: System position and motor position, denoted by X and θ. Their first time derivatives $\dot{X}$ and $\dot{\theta}$, account for linear and angular velocity. And the second ones $\ddot{X}$ and $\ddot{\theta}$ for linear and angular acceleration.

Lagrangian:

$$\frac{\partial}{\partial t}\left(\frac{\partial T}{\partial \dot{q}_j}\right)-\frac{\partial T}{\partial q_j}+\frac{\partial V}{\partial q_j}+\frac{\partial D}{\partial \dot{q}_j}=Q_j \tag{1}$$

Kinetic Energy

$$T=\frac{1}{2}m\left\|v_m\right\|^2+\frac{1}{2}\cdot M\cdot \dot{x}^2 \tag{2}$$

Where $\|v_m\|$ is the eccentric mass velocity, defined as:

$$\left\|v_m\right\|=\sqrt{(\dot{x}-l\dot{\theta}\sin\theta)^2+(l\dot{\theta}\cos\theta)^2} \tag{3}$$

From **Eq. 2** and **Eq. 3** we can obtain:

$$T=\frac{1}{2}m\left\|v_m\right\|^2+\frac{1}{2}\cdot M\cdot \dot{x}^2=\frac{1}{2}m\left[(\dot{x}-l\dot{\theta}\sin\theta)^2+(l\dot{\theta}\cos\theta)^2\right]+\frac{1}{2}M\cdot \dot{x}^2$$

$$T=\frac{1}{2}m\left[\dot{x}^2+l^2\dot{\theta}^2-2l\dot{x}\dot{\theta}\sin\theta\right]+\frac{1}{2}M\cdot \dot{x}^2 \tag{4}$$

Potential Energy

$$V=\frac{1}{2}K_{muscle}x^2+\frac{1}{2}K_{skin}x^2=\frac{1}{2}\cdot(K_{muscle}+K_{skin})\cdot x^2 \tag{5}$$

Dissipative Energy

$$D = \frac{1}{2} C \cdot \dot{x}^2 \tag{6}$$

The variables or DoF of our system are associated to either a force or a torque, accounted as Q_j in the Lagrangian (**Eq. 1**). In our case we only have a torque (**Eq. 7**) which is related to variable θ. It is exerted by the dc motor, and it can be obtained through the dc motor equation [10]. The constants in this equation are explained in further detail in 2.2.4.2.

$$\tau = V \cdot \frac{K_t}{R} - \left(v + \frac{K_b \cdot K_t}{R} \right) \tag{7}$$

Because in this work we use Matlab for our simulations, we convert our ordinary differential equations (ODEs) to state space form which facilitates implementation of Matlab's numerical method. We found that the ODE15s solver is the most suitable one for our case due to its low to medium level of accuracy. We are also interested in running many simulations and a more accurate solver would take too much computational time and effort.

$$\begin{pmatrix} x(1) \\ x(2) \\ x(3) \\ x(4) \end{pmatrix} = \begin{pmatrix} \dot{x} \\ x \\ \dot{\theta} \\ \theta \end{pmatrix} \tag{7};$$

$$\begin{pmatrix} \dot{x}(1) \\ \dot{x}(2) \\ \dot{x}(3) \\ \dot{x}(4) \end{pmatrix} = \begin{pmatrix} \ddot{x} \\ \dot{x} \\ \ddot{\theta} \\ \dot{\theta} \end{pmatrix} = \begin{pmatrix} \ddot{x} \\ x(1) \\ \ddot{\theta} \\ x(3) \end{pmatrix} \tag{8}$$

Figure 3: State space representation suggests that we need to solve our two ODEs, found applying the Lagrange's method, for system acceleration and motor angular acceleration. Spaces 1x1 and 1x3 in matrix **Eq. 8** respectively.

Finally, the mathematical model of our system is given by the following expression (**Eq. 9**) in state space form. The solution of these equations will define the dynamics of our system (**Figure 2**). ODE15s will return variables x(1), x(2), x(3) and x(4) (**Eq. 7**), as a function of time. The behavior of these parameters will be studied in further stages of this work by introducing K_{Muscle}, K_{Skin}, C_{Skin} as variables and also optimized for m, l and V.

$$\begin{cases} \dot{x}(1) = \dfrac{\dfrac{m \cdot l \cdot \sin x(4)}{m \cdot l^2 + J} \cdot \tau + m \cdot l \cdot x(3)^2 \cos x(4) - (K_{Skin} + K_{Muscle}) \cdot x(2) - C \cdot x(1)}{m + M - \dfrac{(m \cdot l \cdot \sin x(4))^2}{m \cdot l^2 + J}} \\ \dot{x}(2) = x(1) \\ \dot{x}(3) = \dfrac{\tau + m \cdot l \cdot \sin x(4) \cdot xdot(1)}{(m \cdot l^2 + J)} \\ \dot{x}(4) = x(3) \end{cases} \tag{9}$$

2.2.1 Muscle Stiffness

Muscles produce two kinds of force by contracting their fibers, active and passive, which sum to compose a muscle's total force. This action has been largely modeled using a Hill's model (**Figure 4**). The model is composed of three elements: Contractile element (CE) which is the element in charge of generating force, an elastic element in parallel with the contractile element (K_{PE}), which is responsible for the muscle passive behavior when it is stretched, and a series elastic element (K_{SE}), which represents the tendon.

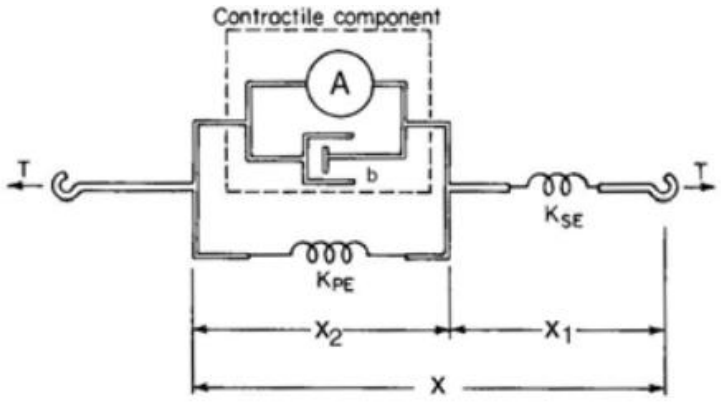

Figure 4: Hill's muscle model considering three elements: Contractile component (CE), parallel elastic element (K_{PE}) and series elastic element (K_{SE}).

In our model, the stiffness that we take into consideration is a mixture of the parallel elastic element (K_{PE}) and the series elastic element (K_{SE}). Thus, for us K_{Muscle} defines the total muscle stiffness measured, combination of the series and parallel elastic elements.

Muscle stiffness is considered as a variable in our simulations, since it defines muscle activity. For instance, if we are holding a cup of coffee and if we want to hold it more firmly, K_{Muscle} will have to increase, hence the strength in our hand will become higher and as a consequence the cup of coffee will be squeezed stronger, and vice versa.

Eventually, one of our purposes in this work is to determine muscle stiffness using our device by correlating it with motor velocity. As a gold standard, we estimated skin stiffness from grip force by usingdata from a previous experiment that used an interposed actuator to measure grip stiffness [4]. From this data we picked the subject who was capable of producing the largest force/stiffness. In terms of computer simulation, since this previous research showed that the relationship between stiffness and grip force is essentially linear, K_{Muscle} is defined as an input and introduced as a linear vector of size 1x40, and bounds at $K_{MuscleMIN} = 1$ and $K_{MuslceMAX} = 816.1$.

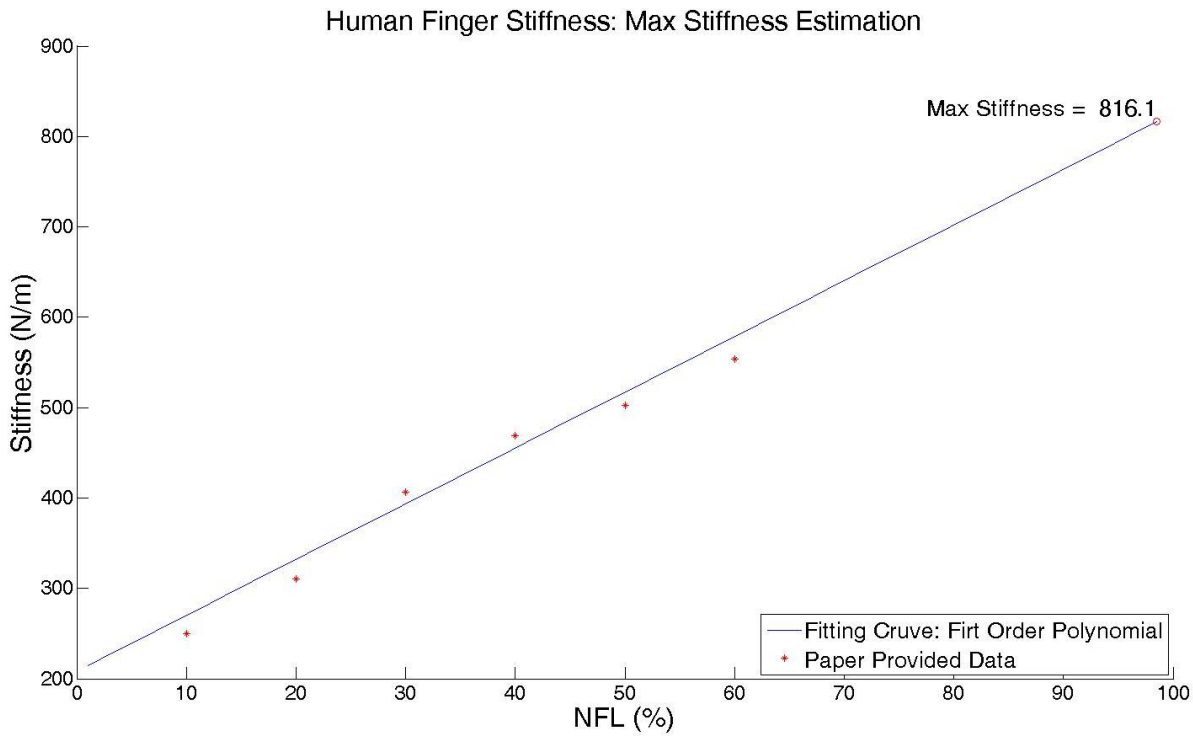

Figure 5: Graphical representation of the estimated stiffness and Normalized Force Level NFL, interpolated for the whole range of force. At the maximum force level 100%, we have a muscle stiffness of 816.1 N/m. Graph taken from [4], Fig. 4, subject B.

2.2.2 Skin Mechanical Impedance

Skin mechanical impedance properties have to be taken into consideration since it is very well known that they can vary for many reasons.

- Skin is compressed due to its springy component: the higher the compression the larger the impedance.

- As a results of vibrations [2]: Something more complex happens in this case, since some different behaviors or properties can be shown depending on the part of our body where we want to focus our action. For example, on the human hand, it has some considerable variations. Natural frequencies can be found within 80-200 Hz. At the start (i.e. for low frequencies) the impedance decreases with the frequency down to a minimum level, after which it increases. This minimum level defines resonance, *fr*. The viscous parts of the skin tissues are where the absorption of vibration is going to take place. The mechanical vibration is transformed into heat defining the damping component.

- Hence, skin mechanical impedance is also going to be dependent on diameter of skin affected by vibration. The more area affected the larger is the effect [1],[2].

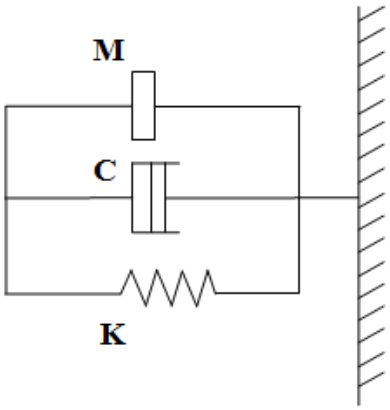

Figure 6: scheme showing skin mechanical impedance. Composed of a mass component (M), a damper component (C) and a spring component (K) which represents stiffness. All of them in parallel with each other.

Despite the fact that skin is highly non-linear, modeling it as a linear system is a reasonable assumption for our case [3]. So, for our simulation (2.4) we define skin stiffness and damping as linear functions that go from an initial to a final value.

The estimation of this impedance was made using [2] and [3], and introduced as vectors of size 1x40, with bounds at:

- Skin Stiffness [N/m]: 25-4200
- Skin Damping [N-s/m]: 1-17
- Skin Mass [g]: 2.4 constant.

2.2.3 System Total Mass

The total mass of our system is the sum of the off-balance load, dc motor, ring and finger mass. The dc motor mass is provided by the manufacturer, the off-balance load and ring mass can be obtained by weighting them on a scale. On the other hand, to find mass of the finger, the density and volume of it were estimated by considering the bone density of the finger (ρ_{Bone} = 1.1 g/cm^3 [8]) and approximating its volume to a cylinder.

$$M_{Finger} = \rho_{Bone} \cdot V_{Finger} \tag{10}$$

Next, the finger is contemplated as a spring element in a cantilever configuration [9].

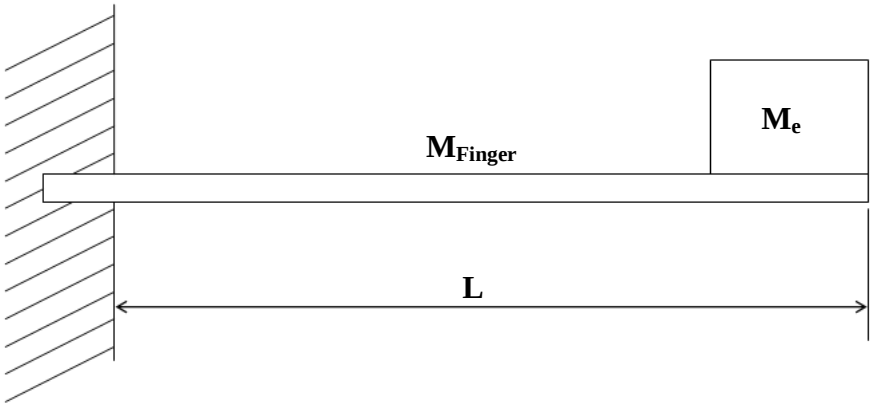

Figure 7: Cantilever configuration of the finger. Where M_e is the mass of the dc motor, off-balance load and ring enclosure, and M_{Finger} is the finger mass. This model allows us to find the equivalent mass of the system M_1.

To determine the equivalent mass, the basic idea is to find a unique mass that placed at the end of the beam gives us an equivalent system in terms of kinetic energy, in other words it is called kinetic energy equivalence. The formula applied is:

$$M_1 = M_e + 0.23 \cdot M_{finger} \tag{11}$$

Eventually, to find the total mass of the system all we have to do is to add the mass of the skin (M_2):

$$M = M_1 + M_2 \tag{12}$$

Table 1: Masses in our system, with **Eq. 11** and **Eq. 12** it gives us a total mass of ≈ 16 g.

System Mass			
Parameter	**Description**	**Measurement Method**	**Value [g]**
M_{DC}	DC motor mass	Given by manufacturer	2.4
m	Off-Balance Load mass	see 2.2.4	see 2.2.4
M_{Finger}	Index finger mass	See 2.1.3	6.9
M_{Ring}	Ring Mass	Scale	12

2.2.4 Eccentric Mass DC Motor

In our study we used a pager motor by SolarBotics. We decided to use this motor for our study because they are very economic, efficient and it satisfied our requirements size wise. Also, it is a popular dc motor used in many applications. That means that is versatile and robust.

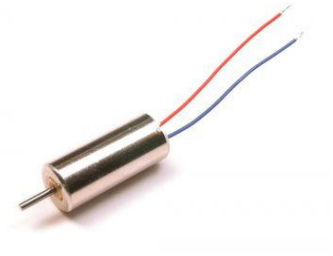

Figure 8: Regular pager dc motor by SolarBotics. It measures in at 7.05mm (0.277") diameter, 16.54mm (0.651") body length, and 21.7mm (0.854") overall length, with the shaft diameter of 1.01mm(0.039").

Not so many performance features are given by the manufacturer, but enough to build our dc motor model and figure out the value for all the parameters that appear in these equations of motion.

Table 2: Regular pager dc motor characteristics. 1.5V gives 17.5mA free draw current (120mA stall) at 9700RPM. 3V gives 22mA free (260mA stall) at 18,420RPM. 5V operation give 32.1mA free (420 stall) at 31,900RPM.

Voltage	RPM	Current (free)	Current (stall)
1.5V	9700	17.5mA	120mA
3.0V	18420	22mA	260mA
5.0V	31900	32.1mA	420mA

2.2.4.1 Off-balance load

In order to off-balance the system and create the vibration, we manufactured our own eccentric mass which mounted onto the motor's shaft acted as an eccentric load. In like manner, manufacturing it allowed us to add/remove weight when desired, hence control the vibration. So, the level of vibration is dependent on our own off-balance load (2.2.4.1) and on the level of electric power supplied (2.3.1.1) to the dc motor as well, which determined by the voltage that we control sets the motor at different speeds.

We essentially; used two different off-balance setups. The first one was meant to create a big off-balance vibration and the second one to create a smaller effect. The design of this load was very simple. A cylinder with a bore to press-fit the shaft of the dc motor and act as a coupling in order to later on twist three screws in the sides, perpendicularly to the shaft where three more bores had been made and tapped beforehand. The purpose of these screws was to create an off-balance movement, as well as making sure that the motor's shaft and coupling spin together, hence the lowest one (see **Figure 9** and **Figure 10**), acts as a set screw by compressing the shaft. Their size is 2/56", so we are dealing with small stuff and we do not need light weights. The material used for the coupling was PTFE-Filled Delrin® Acetal Resin, by performance plastic.

In this section, the parameters of interest for us are mass (in grams) and eccentricity (in millimeters). Thus, a SolidWorks model of the off-balance load helped us to figure them out by evaluating the mass properties of the assembly. Density was assigned to each component, and the Cartesian origin was placed at the center of the coupling so we could directly obtain the eccentricity.

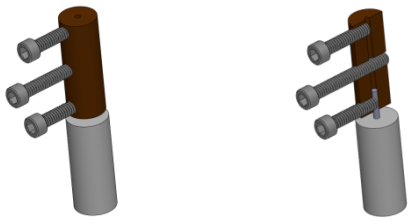

Figure 9: Picture showing SolidWorks assembly. Whole and partial views of the first setup. DC mass eccentric motor plus off-balance load which consists of three 2/56" screws and coupling. This assembly was designed to create a high vibratory effect to our system.

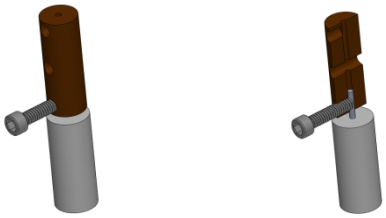

Figure 10: Picture showing SolidWorks assembly. Whole and partial views of the second setup. DC mass eccentric motor plus off-balance load which consists of one 2/56" screw and coupling. This assembly was designed to create a low vibratory effect to our system.

Table 3: Values of off-balance load and eccentricity for sets one and two.

Parameters	**m** (off-balance load) in grams	**l** (eccentricity) in mm
SETTING #1	1.89	4.25
SETTING #2	1.01	2.11

2.2.4.2 DC Motor model

The behavior of our system depends on the characteristics of our dc motor. It determines velocity, torque and power. Hence, it was very important to build a very accurate model of it. Parameters such as rise time, time constant, bandwidth and final motor velocity may be a little off with respect to the reality unless we achieve a good modeling for our dc motor.

The equations of motion for DC motors are (Eq. 13):

$$\begin{cases} V = L\dfrac{dI}{dt} + RI + K_b\dot{\theta} \\ J\ddot{\theta} = K_t I - v\dot{\theta} - \tau \end{cases} \qquad (13)$$

where, V is the voltage applied to the motor, L is the motor inductance, I the current through the motor windings, R the motor windings resistance, K_b the motor's back electromagnetic force constant, $\dot{\theta}$ the rotor's angular velocity, J the rotor's moment of inertia, k_t the motor's torque constant, υ the motor's viscous friction constant, and τ the torque applied to the rotor by an external load. However, the dc motor behavior will be analyzed at the two equilibrium points, taking advantage of the fact that we are given the characteristics of our dc motor for three different voltages (**Table 2**):

- Stall: when the load carried by the dc motor is so large that the angular velocity goes down to zero, essentially because the motor cannot handle so much torque.
- Free: when there is no load carried by the dc motor and it turns without any resistance.

The system is called to be in equilibrium when after applying a voltage, the motor angular velocity settles (i.e. reaches a steady value). The motor is not accelerating anymore and the current drawn by it has stabilized, so the derivatives in **Eq. 13** are zero. Hence, taking all that into consideration, and the fact that if there are no electromagnetic losses, the torque constant is equal to the motor's back electromagnetic force constant and then we can assume [12]:

$$K_b = K_t \tag{14}$$

The equations of equilibrium are:

$$\begin{cases} V = RI + K_b\dot{\theta} \\ \tau = K_t I - v\dot{\theta} \end{cases} \tag{15}$$

Table 4: DC Motor variables calculated using **Table 2**, **Eq**. **14** and **15**. Motor winding resistance measured using a multimeter, and for the motor moment of inertia we picked a low value since it is very insignificant compared to the off-balance load mounted onto the shaft.

DC MOTOR			
Parameter	**Description**	**Value**	**Units**
Kb	Motor's back electromagnetic force constant	0.00135	V·s/rad
Kt	Torque constant	Kt = Kb	N·m/Amp
v	Motor's viscous friction constant	$1.71 \cdot 10^{-8}$	N·m·s/rad
R	Motor winding resistance	18	Ohms
J	Motor moment of inertia	$5 \cdot 10^{-9}$	$Kg \cdot m^2$

2.2.4.3 DC Motor performance characteristics

In this section we show a simulation of our DC motor performance characteristics, considering that it carries no load: m = 0 g (**Figure 2**).

Table 5: DC Motor simulation parameters for V = 1.5 volts.

Voltage	RPM	Current (free)	Current (stall)
1.5V	9553	15mA	127mA

As we can observe in **Table 5**, the parameters of the simulation that we obtained are very close to the ones provided in **Table 2**. Hence, we can consider that the model build of the dc motor is good enough.

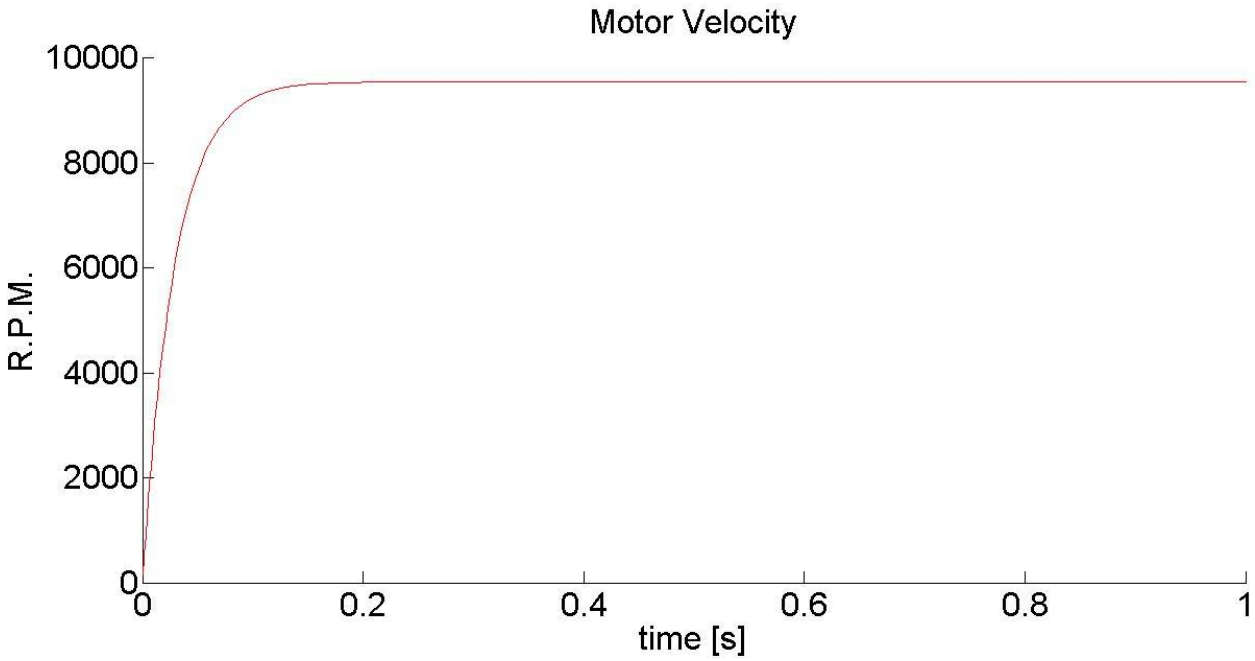

Figure 11: Motor velocity characteristic curve. Where the settling time is $\tau_s \approx 0.2$ s and motor velocity at equilibrium point 9553 R.P.M.

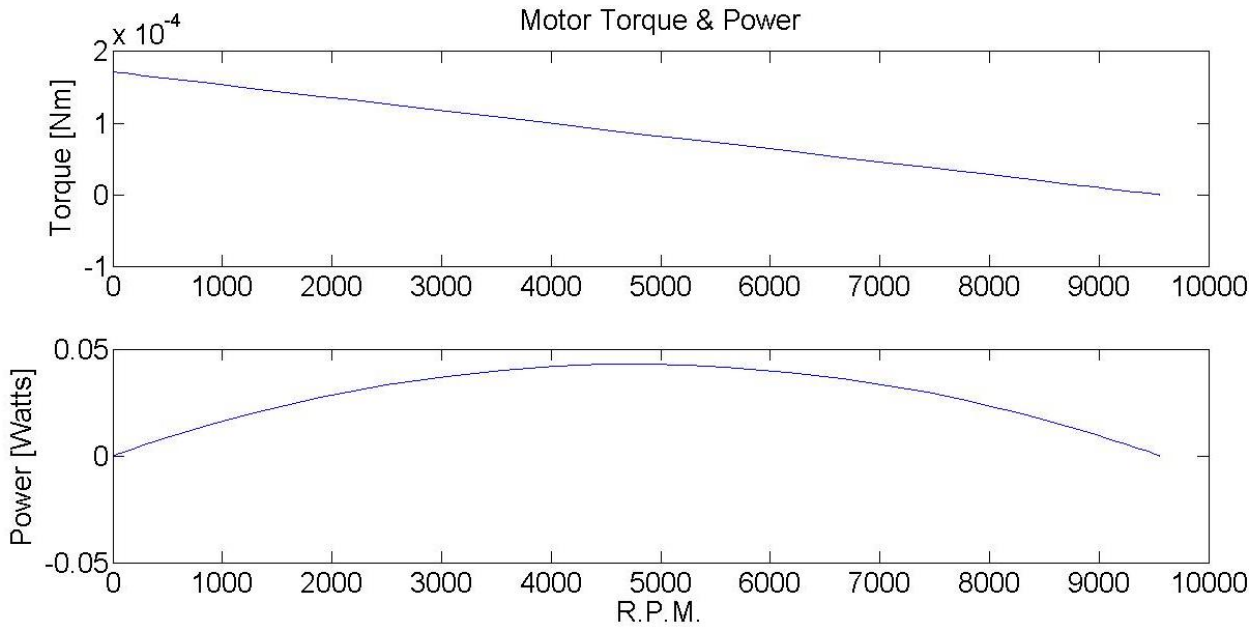

Figure 12: Torque and power characteristic curves, with a maximum torque of 0.1716 Nmm and a power peak at 43 mW.

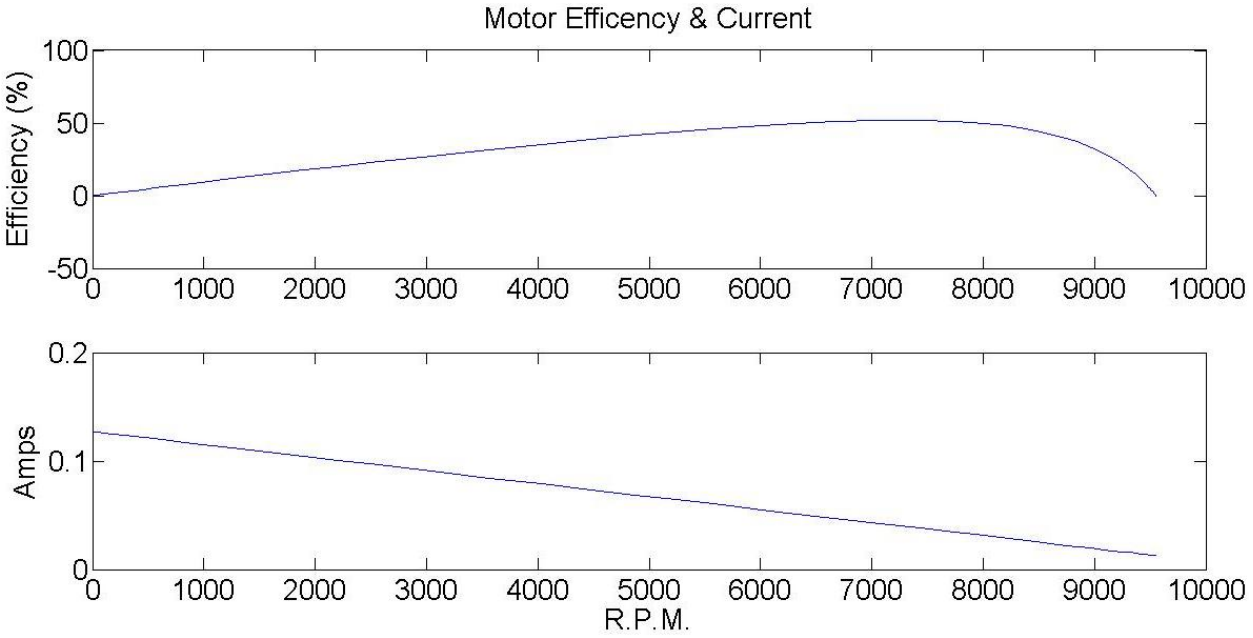

Figure 13: Efficiency and Current characteristic curves, with efficiency peak at 52 % and with maximum current at 127 mA.

2.3 Experiment Setup

In this section we describe the two experiments we conducted in order to verify our hypothesis, as explained in 2.1.

First of all, the idea is to show that stiffness can be written as a function of motor velocity for our type of system. Hence, we came up with a simple system, a cantilever beam with variable length, which can allow us to find a clear correlation between parameters, and in the same manner was easy to model. Also, it is a quite studied case so that a lot of information can be found about it. The dc motor was mounted to the free end of the beam. Different lengths were defined which cause different levels of stiffness. Then, starting by setting the beam at a long span, progressively we shortened it as we measure the velocity of the motor for each given length or level of stiffness, eventually building a graph with the measurements obtained. This procedure was repeated for three different voltages and two off-balance loads, so we can investigate the behavior of our eccentric mass dc motor for different settings. The voltage was controlled by connecting it to a Laboratory DC Power Supply *HY3005D,* which allowed the adjustment of output voltage. Also two other magnitudes were measured, motor velocity and vibratory acceleration. The most suitable device to collect this type of data is an accelerometer. Hence frequency of vibration (which is equivalent to motor velocity) and vibratory acceleration can be read. In addition, we made use of a stroboscope to measure motor velocity so accelerometer readings can be supported.

Secondly, we also needed to show that an actual ring sensor could be built and that we could use its principle of operation to measure grip force and muscle stiffness. For this reason, a

rudimentary ring sensor was put together. Composed of a flexible ring made of electrical tape and paper, it supported the eccentric mass dc motor on the outside. It is easy to pun on and take, off the index finger. The ring is also comfortable and light weight, which are important requirements so the subject who wears it is not supposed to notice anything. The same instruments utilized for the cantilever beam setup were used here for taking measurements, an accelerometer and a strobe light. Furthermore, a force transducer to demonstrate direct correlation between motor velocity and grip force was used as well.

The data obtained was acquired using a national instrument, NI USB-6009 and processed with Matlab.

2.3.1 Experiment Equipment

2.3.1.1 Power supply

The regular pager dc motor voltage can be controlled by connecting it to a Laboratory DC Power Supply *HY3005D.* The current drawn is dependent on voltage and load mounted onto the shaft. Those are input parameters for us, which we require to be constant for each experiment. The current on the dc motor will also drop as it speeds up due to an increase in muscle stiffness/grip force which will provoke a decrease in system inertial load. The apparatus is equipped with LCD Displays for voltage and current, however a multimeter was used to double-check voltage output, since resolution was not accurate enough. Some features: Input Voltage: 207 - 253V AC, 50Hz. Output Voltage: 0 - 30V DC. Output Current: 0 - 5A DC.

2.3.1.2 Accelerometer

A MMA7361L 3-Axis Accelerometer ±1.5/6g by Polulu was used. This device was highly suitable for both of our experiment setups due to its tiny dimensions. It is a low-g accelerometer, with maximum sensitivity range of 6g, which is within our range of study, considering that we are not interested in studying high levels of vibration because we want our wearable ring sensor to be a comfortable for the subject. This device also allowed us to measure frequency, since the output is an sinusoidal curve with amplitude equal to acceleration in g (9.81 m/s^2).

2.3.1.3 Stroboscope

A strobe light capable of emitting up to 12,215 flashes per minute was used to measure motor velocity. It is done by matching flashing rate emitted by the stroboscope with the speed of rotation of the motor. So, out of this measurement we can obtain directly revolutions per minute. Our off-balance load allowed us to use this instrument since the screws could be taken advantage of as a reference. Eventually, we wanted our screws to standstill which meant that flashing rate and motor velocity matched.

2.3.1.4 Force transducer

Composed of a handgrip and a load cell, the force transducer provided us direct grip force measurements by squeezing the handgrip, using a NI 6221 DAQ for acquiring the data and ultimately Matlab for processing it.

2.3.1.5 Data acquisition

National instruments NI USB-6009 and NI 6221 DAQ were used to acquire data from the accelerometer and force transducer respectively. Equipped with several analog and digital ports for receiving inputs and sending outputs. These national instruments were very convenient for our study, also easy to set up and use since NI-DAQ drivers is the only thing needed to allow Matlab read from them.

2.3.2 Cantilever Beam Experiment

The main requirement for our cantilever beam was a variable length, hence a slider anchored with a bar clamp at one end formed the support, capable of withstanding the moment and shear stress produced by the eccentric mass motor vibration. The span of the beam could be varied by loosening four straps. Nevertheless, during the experiment the end of the beam was strapped tight in order to ensure the proper cantilever behavior of the system. The eccentric mass motor was located at the free end, supported by a plastic connection mounted to the beam. The accelerometer was attached at the end of the beam as well, right next to the eccentric mass dc motor. Its axis was perfectly aligned with the system, so meaningful measurements could be obtained. Essentially, the z axis was the one oriented towards the vibration direction, y axis was parallel to the longitudinal axis of our beam and x axis parallel to the revolution axis of the dc motor.

The beam material was brass with a transverse section of 1.61x25.6 mm^2 and a density of 8500 kg/m^3. The mechanical properties of brass are very well know, however since sometimes there can be little variations, we carried out an experiment to figure out the Young's Modulus (E). A weight of 1.073 Kg, was hanged from the free end of the beam for different lengths. Each desired stiffness was represented by a length which was calculated using **Eq. 16** [9].

- Stiffnesses considered in N/m: 1500, 3000, 4500, 6000, 7500, 9000, 10,500, 12,000.
- Respective lengths in mm: 119.4, 94.77, 82.79, 75.22, 69.828, 65.71, 62.419, 59.70.

Deflection was measured. Then, using **Eq. 17** [9] the Young' Modulus was computed for each case. Eventually, the average was taken to determine the final value of E using the value of E_i for each length or stiffness level. Hence, the Young's Modulus obtained was 95,753.28 MPa, which is very close to the value found in books.

$$K = \frac{E \cdot w \cdot h^3}{4L^3} \tag{16}$$

$$\delta = \frac{P \cdot L^3}{3 \cdot E \cdot I} \tag{17}$$

2.3.2.1 Experiment procedure

The wires of the dc motor were connected to the positive and negative ports of the power supply using two bananas. Thirteen levels of stiffness were defined. Starting at low values and ending at high stiffnesses. Hence, from long spans to short ones:

K_{SYSTEM} [N/m]= [250, 500, 625, 750, 1000, 1500, 3000, 4500, 6000, 7500, 9000, 10500, 12000].

Acceleration measurements were taken during ten seconds for every stiffness considered. The Matlab routine to obtain data was started a little bit before than the dc motor. In that manner, we could see the transition of our system from standstill to nominal conditions of operation for the

settings chosen. Meanwhile motor velocity was checked with the strobe light. Next, the straps were loosened, the beam slid out on to the next stiffness, and so forth.

The procedure was repeated three times for three different sets of parameters since we are also interested in studying the dependency of the system on voltage and off-balance inertial load. In conclusion, we were taking motor velocity and vibratory data thirteen times per experiment (since we defined thirteen stiffnesses).

- EXPERIMENT #1: V = 0.75 v, m = 1.01 g and l = 2.11 mm
- EXPERIMENT #2: V = 1.5 v, m = 1.89 g and l = 4.25 mm
- EXPERIMENT #3: V = 2.0 v, m = 1.01 g and l = 2.11 mm

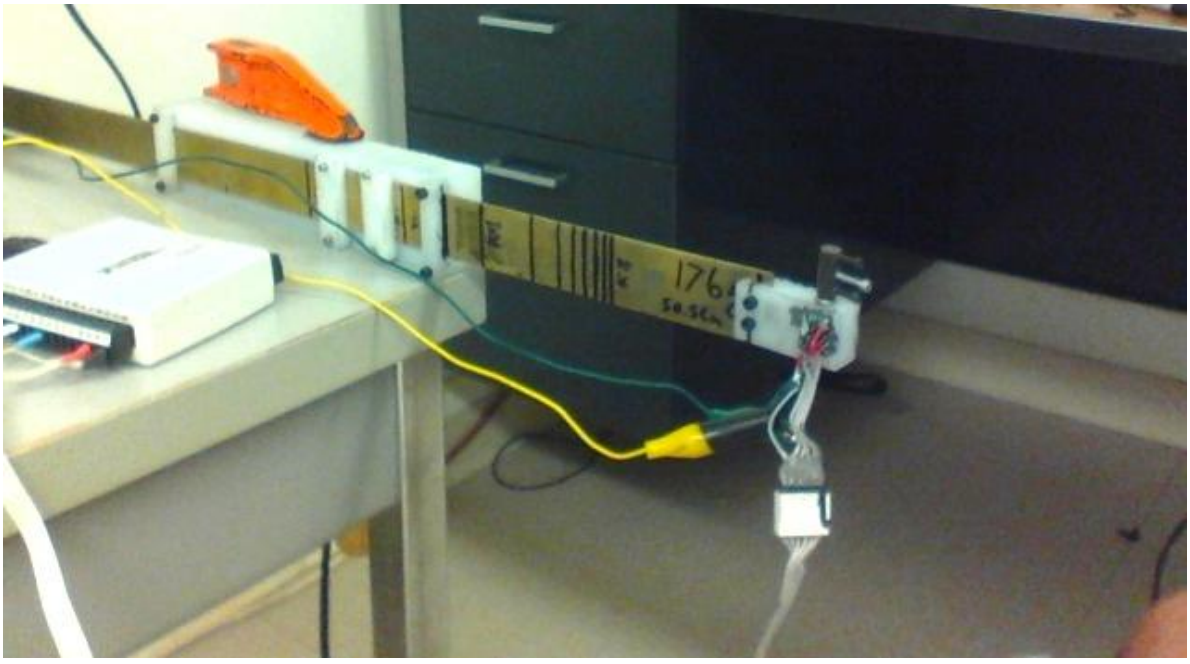

Figure 14: Cantilever beam setup. Eccentric mass dc motor is standstill. The beam was slid in and out in order to change the stiffness and measure the vibration and speed of the dc motor.

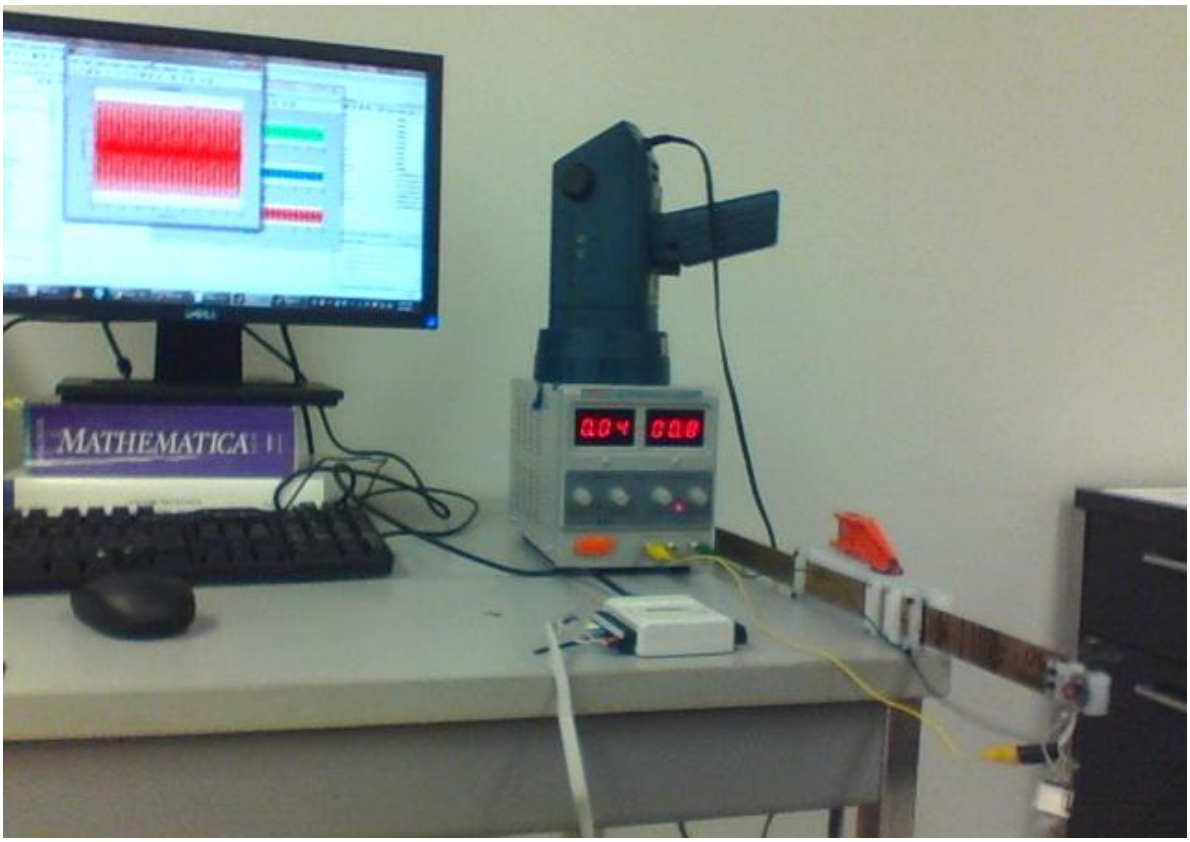

Figure 15: Picture of the whole cantilever beam setup. On the right, beam anchored to the table, eccentric mass dc motor rotating. In the middle, national instrument, stroboscope and power supply. On the left side of the picture, computer with Matlab acceleration data plots.

Find a video of the experiment in Appendix **Error! Reference source not found.**.

2.3.2.2 Cantilever beam model

The dynamic model for the cantilever beam system was considered **Figure 16**, in order to obtain the right behavior in our simulation and to be able to compare simulation vs. experimental data. It is slightly different than the model for the ring sensor 2.2. It is composed of one spring,

damper and mass. All of them are properties of the material/beam, which vibrate due to the action of the eccentric mass motor, whose model, of course, is not going to change.

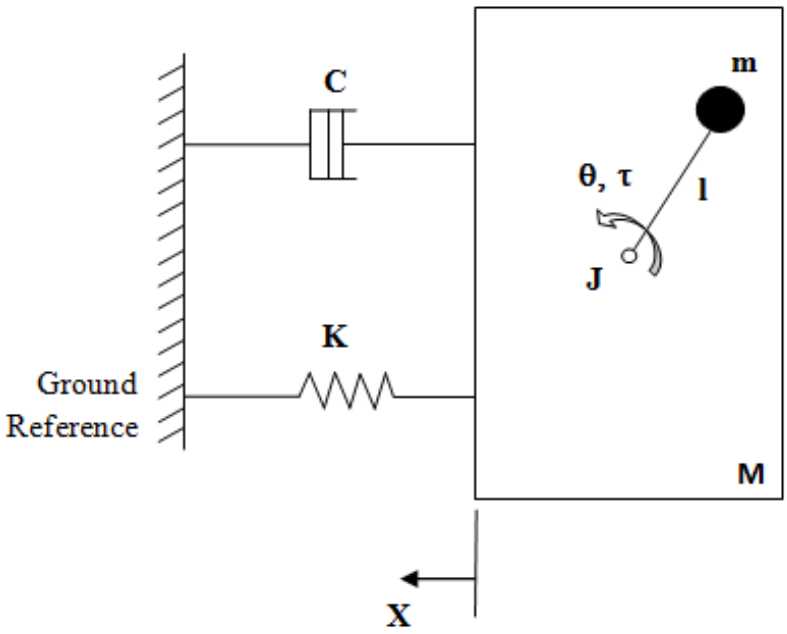

Figure 16: Cantilever beam model.

System total mass will vary for every level of stiffness since the more length the more mass, and vice versa. Again, we will have to find the equivalent mass using 2.2.3 and adapting it to new system. First of all, we can know the mass introduced by the material for every given length multiplying volume times density. Also the mass of the other components in the system can be found either by weighting them on the scale or using provided data. So, the weight of the dc motor is given, its support mounted to the end of the beam can be weighted and off-balance load is also an already known parameter. Hence, system mass can be identified.

Table 6: Beam total mass for each stiffness level.

K [N/m]	250	500	625	750	1000	1500	3000	4500	6000	7500	9000	10,000	12,000
M_{SYSTEM} [g]	34.7	31.5	30.7	30	29	27.8	26.1	25.2	24.7	24.4	24.1	23.8	23.6

The only parameter that we are missing is damping, which is usually the hardest to determine. The idea is to figure it out by applying and impulse to the beam for each level of stiffness considered and then fit an impulse response **Eq. 18** [9], to the actual data which can be obtained with the accelerometer.

$$y(t) = \frac{\omega_n}{\beta} \cdot e^{-\omega_n \cdot \xi \cdot t} \cdot \sin(\omega_n \cdot \beta \cdot t + \varphi) \tag{18}$$

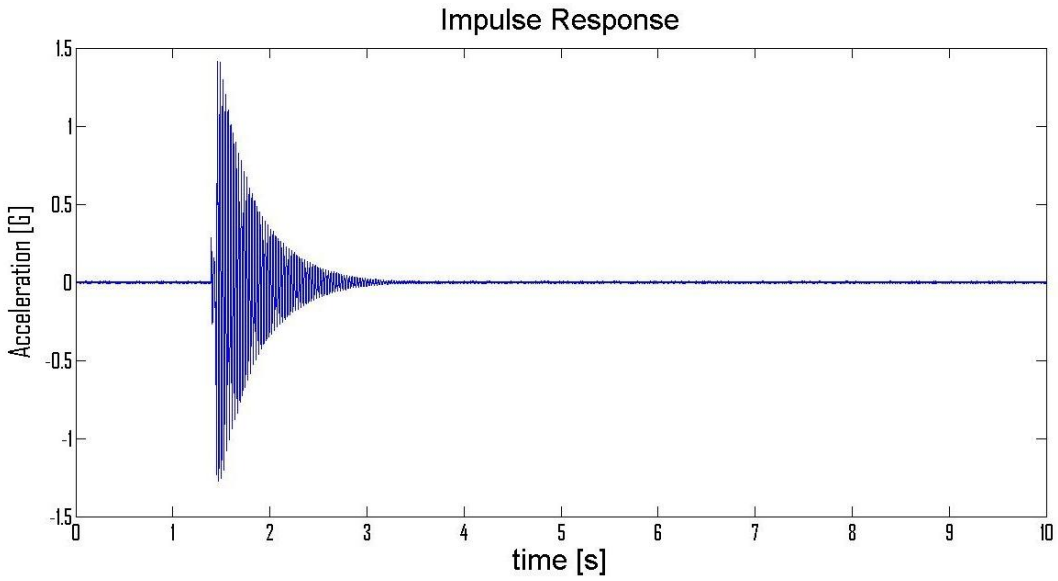

Figure 17: Impulse response for a span of 119.4 mm or 1500 N/m.

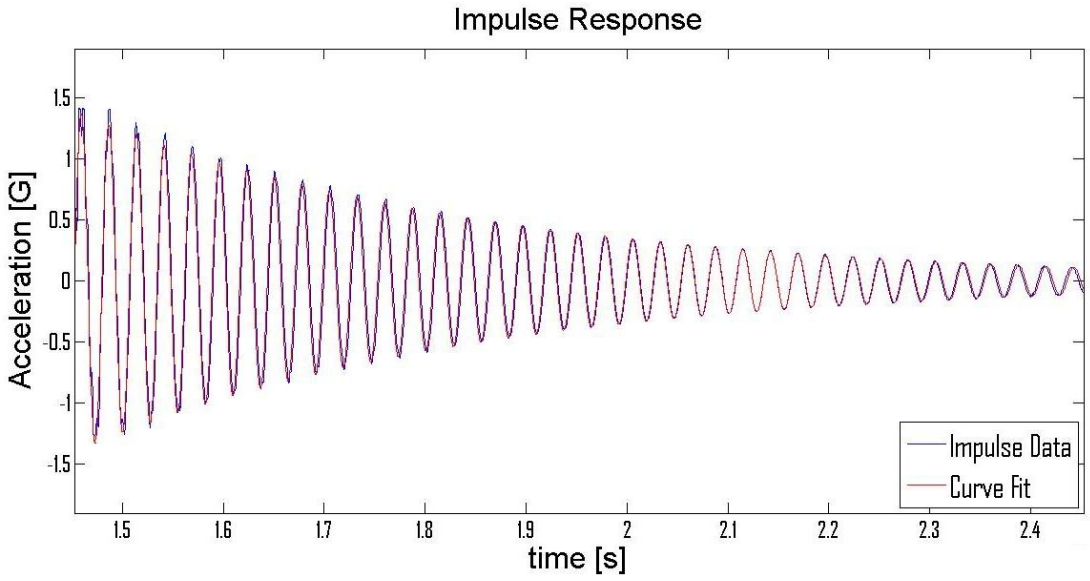

Figure 18: Impulse response fit curve for stiffness 1500 N/m. Both curves overlap, meaning that the fit is good.

Process showed in **Figure 17** and **Figure 18** is repeated for every level of stiffness. After fitting the impulse responses, we can obtain the value of damping ratio for each stiffness, K. It is just a matter of comparing coefficients (**Eq. 18**) given that we know the mass of the system, hence natural frequency can be found, $\omega_n = (K/M)^{1/2}$.

Ultimately, through damping ratio we can calculate damping constant C, by applying **Eq. 19**, for every level of stiffness.

$$\xi = \frac{C}{2\sqrt{K \cdot M}} \qquad (19)$$

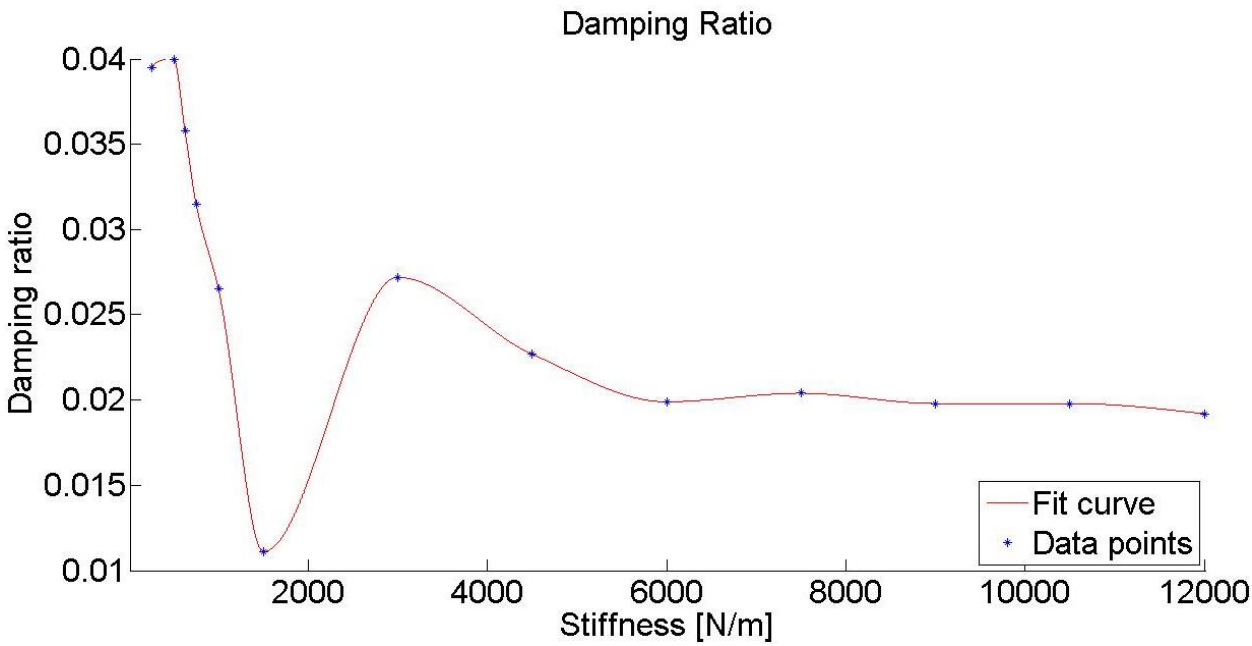

Figure 19: Damping ratio evolution for thirteen levels of stiffness considered. In N/m: 250, 500, 625, 750, 1000, 1500, 3000, 4500, 6000, 7500, 9000, 10,500 and 12,000.

The fit curve in **Figure 19** is an interpolation so we can know the damping ratio for any given level of stiffness. It goes down, for stiffnesses near resonance of the system, at stiffness 1500 N/m, and then after 6000 N/m it settles.

2.3.3 Ring Sensor Experiment

A rudimentary ring was build to demonstrate the validity of our approach. It is a non-contact grip force sensor. The most important feature of our device with respect to other vibratory apparatus is that ours is not in touch with the skin, although the skin is affected by the vibration. It is not inserted between the object and the finger. Therefore, the ring mounts the eccentric mass motor facing the outside of the hand.

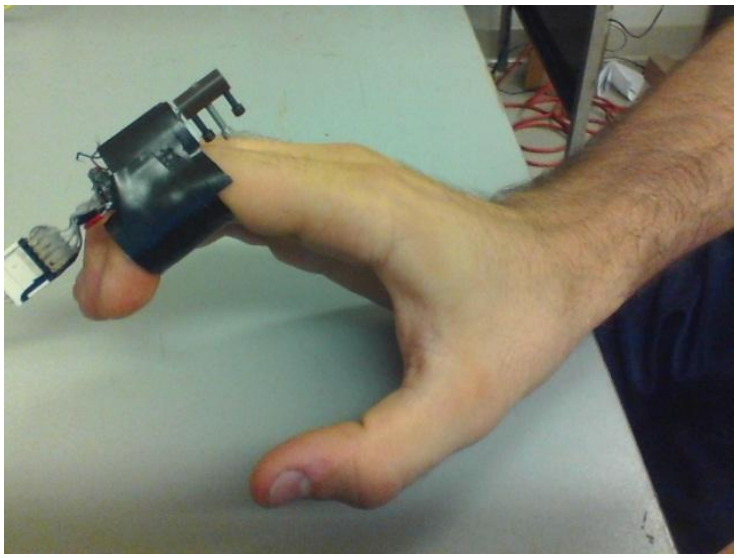

Figure 20: Picture of the non- interposed ring sensor setup. The subject is wearing the device on the intermediate phalange of the index finger

2.3.3.1 Experiment procedure

The experiment carried out here was simpler than the cantilever beam experiment, 2.3.2. The goal was to show a direct dependence between motor velocity and grip force, ultimately, relating this grip force to muscle stiffness using [4]. The only parameter that we wanted to change for this experiment was the off-balance inertial load, which can be easily done by changing the off-balance load setting, 2.2.4. Two experiments were run, one with off-balance load setting #2 and the second with setting #1 (2.2.4.1), always keeping the voltage constant at 0.75 volts. Hence, the purpose was to cause different vibratory effects and see the magnitude of change in the relationship between motor velocity and grip force as we varied the off-balance load.

First of all, the wires of the dc motor were connected to the positive and negative ports of the power supply using two bananas. The accelerometer was glued right next to the dc motor making sure that its axis was aligned. The one oriented towards the vibration direction was X. The handgrip of the force transducer used was squeezed progressively during ten seconds. The basic idea was to start squeezing it very weakly, increase the grade of force applied up to a maximum (NFL = 100%), and then relax the hand again. The procedure was aiming to obtain an acceleration profile that should show, initially a low frequency, continuously increasing to a high frequency and then going back to a low one. Ultimately, the purpose again was to see if the model built in 2.2 exhibited the same behavior as in the reality by comparing simulation vs. experimental data. Both sensors, accelerometer and force transducer, collected data for a period of ten seconds. To make sure that they were synchronized we just started to run their respective Matlab routines at the same time. Finally, all this procedure was repeated two times for each off-balance inertial loading case.

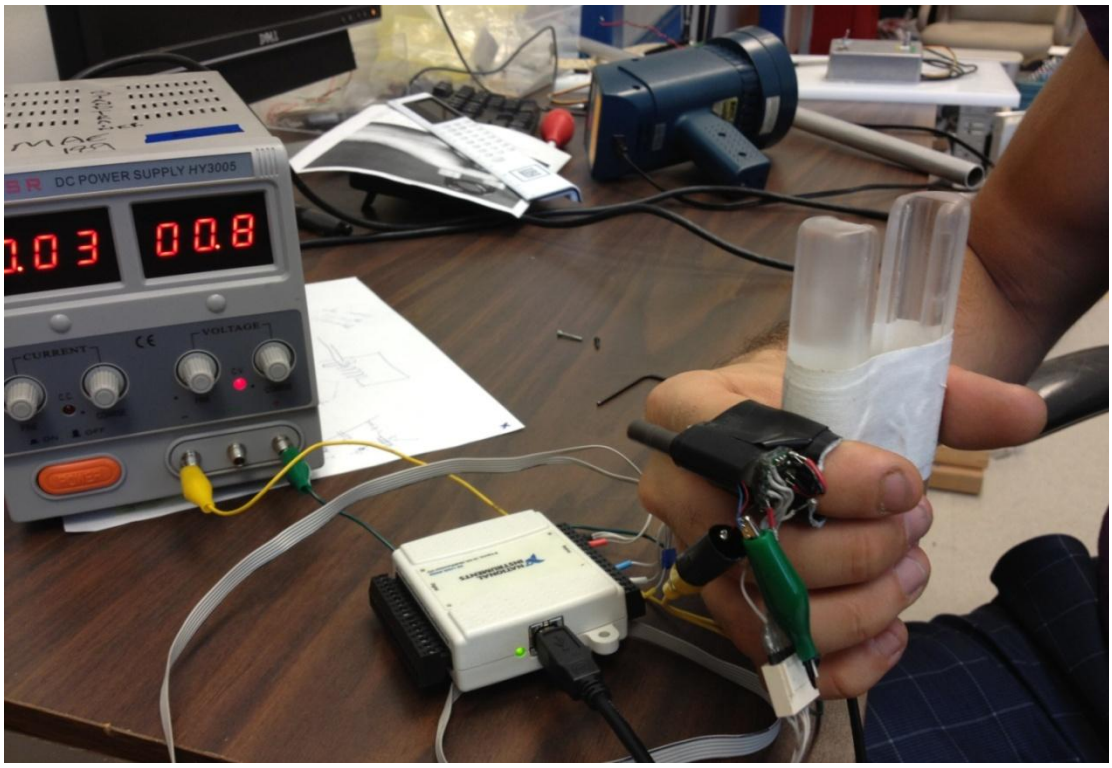

Figure 21: Picture showing ring sensor experiment setup. On the right, force transducer handgrip plus ring sensor worn by the subject. In the middle national instrument to acquire data. On the left side, power supply.

Muscle stiffness 2.2.1, and skin impedance 2.2.2, were considered to be minimum when NFL (%) [4] was right at zero, at the moment right before our finger makes contact with the handgrip. And maximum when NFL (%) [4] was at hundred per cent, i.e. maximum grip force applied.

Find a video of the experiment in Appendix **Error! Reference source not found.**.

2.4 Simulation

In our work, we developed many simulations for several purposes. The main objective was to test the model in order to determine how well it follows reality. The simulation was also a very helpful tool in order to get a good understanding of the physics of our system and see why it follows a particular behavior. Thus, two main simulations, one for each experiment, comparing simulation vs. experimental data were developed. Additionally, four sensitivity simulations were implemented as well, which allow the investigation of the system under the variation of voltage, system total mass and off-balance load. We also want to know for what set of parameters our system exhibits such a behavior that for a change in impedance the frequency of vibration has the steepest increase, and at the same time a low vibration strength. This set of parameters are the optimal ones for our ring sensor. Hence, an optimization routine is presented, which studies many possible combinations for voltage and inertial loading, ultimately picking the optimal.

All the simulations are written in Matlab. All of them consists of two files. In the first one the differential equations (**Eq. 9**) are written and expressed as a function. In the second file we define the input parameters, substitute them into ODE15s solver, it calls the function previously created in the first file and returns four outputs (**Eq. 7)**. Since we intend to model our system as a function of impedance, we will have to define a loop that computes a new input for ODE15s, and it will have to solve the dynamic differential equations for every step or increment returning different outputs. That will demand some computational effort to the computer since the smaller the increments in impedance the more times that ODE15s will be executed.

Firstly, for the cantilever beam experiment, only thirteen steps in stiffness and damping where considered, of varying step size. So stiffness moves in a range from 250 to 12,000 N/m and damping ratio 0.039 to 0.019, (2.3.2.2). For the simulations, the same number of steps was used in Matlab routine developed to compare simulation vs. experiment. However, for the analysis of sensitivity, more steps were computed in order to have more accuracy Stiffness moves in a range from 300 to 10,000 N/m and damping ratio the same, using the interpolation previously made in 2.3.2.2. Also, for all the plots, interpolations between data points were done which gave us a better sense of the evolution or behavior of the system.

Data of system vibratory acceleration vs. stiffness were also analyzed for experiment #1. That helped to support the hypothesis stated in this work, 2.1.

Secondly, for the ring sensor simulation we decided to take smaller increments, since the process of obtaining data was less time consuming than in the cantilever beam experiment. Results from a published work [4],[2] were used. Hence, all we had to do was transfer the data to our simulation, (2.2.1 and 2.2.2). Besides we only ran two experiments for grip force vs. motor frequency.

2.4.1 Cantilever Beam Model

2.4.1.1 Experiment vs. model

Reference code: APPENDIX **Error! Reference source not found.**

In this section, the code used to simulate the behavior of the eccentric mass dc motor, as we progressively vary the stiffness of the cantilever beam, is developed. Also, the experimental data is collected and plotted together with the simulation.

The code is structured in a way that allows the selection of the experiment that we want to display. Since three experiments were carried out, with three different settings, (2.3.2). So after selecting it, the simulation builds vectors for all the parameters of the system, and parameters for the dc motor equations of motion. Then, the parameters are substituted into ODE15s, together with a time vector of two seconds, and it does the numerical integration while it saves the output data of the system, when it is settled, in a matrix. This process is repeated for every level of stiffness, which implies a loop. The stiffness ,defined as a vector, is read position by position, hence each step in the loop is a different position in the vector so a consecutive stiffness level.

Next, the Matlab routine builds the vectors of experimental data, with data from the accelerometer (acceleration and period of vibration) and stroboscope.

Out of it we built our plots with simulation and experimental data, and we compared: stiffness vs. motor velocity, time vs. motor velocity, natural frequency vs. motor velocity, and resonance plot which is vibration displacement vs. the ratio between motor velocity and natural frequency.

The vibration displacement X is computed using acceleration maximum amplitude and motor velocity for the experiment, i.e. **Eq. 20**.

$$|X| = \frac{|Acc|}{\omega^2} \tag{20}$$

At last, stiffness is plotted against g-force, i.e. acceleration. A very important plot to see the evolution of the vibration as we vary stiffness. Only done for experiment #1.

2.4.1.2 Sensitivity analysis

Reference code: APPENDICES **Error! Reference source not found.**, **Error! Reference source not found.**, **Error! Reference source not found.**, **Error! Reference source not found.**.

The goal is to obtain plots for the relationship: stiffness vs. motor velocity for variations of a parameter. No experimental data is involved here, only the cantilever beam model simulation. Four different codes were used to make four analysis of sensitivity. First of all, three parameters were analyzed: voltage, off-balance load and system total mass. All of them have the same code structure which is based on a central loop for moving on the stiffness vector and a second one for moving on a vector composed of a progressive variation of the parameter of study. For instance, for the voltage sensitivity analysis we will create a vector of six different voltages and we will obtain a curve of stiffness vs. motor velocity for each voltage. Same thing for off-balance load and system total mass.

Then, we also want to see what happens to the relationship, voltage vs. motor velocity. In other words, for constant levels of stiffness we increase the voltage progressively and check what happens to the velocity.

The parameters used for the equations of motion in each case were:

- Voltage sensitivity: off-balance load 1.01 g, eccentricity 2.11 mm and system total mass 19.5 g.
- Off-balance load sensitivity: voltage 1.5 v, eccentricity 2.11 mm and system total mass 19.5 g.
- System mass sensitivity: voltage 1.5 v, eccentricity 2.11 mm and off-balance load 1.01 g.
- Voltage vs. motor speed: off-balance load 1.01 g, eccentricity 2.11 mm and system mass 19.5 g.

2.4.2 Ring Sensor Model

2.4.2.1 Experiment vs. model comparison

Reference code: APPENDIX *Error! Reference source not found.*

In this section, the code used to simulate the behavior of the eccentric mass dc motor, as we progressively vary muscle and skin impedance (stiffness plus damping) in the ring sensor model, is developed. Also, the experimental data is collected and plotted together with the simulation. Essentially, we intend to collect all the information from point 2.2 and simulate it.

The total stiffness (K_{Total}) considered was the sum of K_{Muscle} and K_{Skin}. Starting at 25 N/m, and moving linearly up to 5016 N/m. The damping went linearly as well from 1 to 17 N-s/m. System total mass remained constant and it was calculated using 2.2.3**.**

The code structure is the same as in **APPENDIX Error! Reference source not found.**, described in 2.4.1. With only two experiments (2.3.3.1).

We built the plots using the data of the simulation plus the experiment in order to compare stiffness vs. motor velocity. And using only the experimental data we plotted grip force vs. motor velocity.

2.4.2.2 Optimization routine

Reference code: APPENDIX **Error! Reference source not found.**

The goal was to obtain the right combination of values for off-balance load, eccentric distance and voltage that optimize our ring sensor. Maximum sensitivity and a low level of vibration are characteristics that will define the optimal one.

Sensitivity, was defined as the combination of parameters that for an increase in stiffness the eccentric mass dc motor had the largest increase in speed. For that reason, it was interesting to determine the natural frequency of the system because resonance was a phenomena that could be taken advantage of on our benefit, since it implies a peak, i.e. a large change in vibratory conditions. Hence, it would help us achieve maximum rate of change in speed if the initial angular velocity of the eccentric mass dc motor was near the natural frequency of the system.

Low vibration strength was desired in order to have a smooth device which does not produce too much annoyance to the person who wears it.

The satisfaction of these two requirements was attained by computing several combinations of parameters. The slope for each case was calculated, which defines the rate of change in velocity, and also the g-force (1 g = 9.81 m/s^2) produced by the vibration. Finally, a trade-off defined our objective function:

$$Trade-off = \frac{Slope}{G-force} \tag{21}$$

The optimal case was the one that maximized **Eq. 21**. It was not necessarily the case with highest slope and lowest g-force, but something in-between that was acceptable.

Some research on vibrators (**Appendix Error! Reference source not found.**) was done in order to understand the normal conditions of operation of an eccentric mass dc motor, i.e. a vibrator. The acceptable range of vibration and speed was investigated, which was strictly related to eccentric load and voltage. In that manner we could adjust the bounds for our optimization analysis, and narrow the possible number of combinations down to only feasible ones. So, essentially after defining bounds for voltage, off-balance load and eccentric distance (**Table 1**), the Matlab optimization routine ran three loops combining parameters for a simulated increase in impedance. In total 200 combinations were computed. Once out of the loop, the less linear behaviors were not taken into account and the best trade-off was picked, i.e. the optimal set of parameters for our ring sensor.

Table 7: Parameters bounds and number of steps taken, which also define the increment size.

Parameter	Minimum	Maximum	Number of Steps
Voltage [volts]	0.5	2.0	8
Off-balance load [g]	0.25	2	5
Eccentricity [mm]	1	3	6

3 Results

3.1 Cantilever Beam Experiment

For the thirteen levels of stiffness analyzed the data was recorded and plotted. We found high motor velocities for very low levels of stiffness. Then, suddenly the motor slowed down to a minimum point near the natural frequency, defined by stiffness and system mass. This was followed by a near linear increase in motor velocity for medium levels of stiffness. Eventually, for a very stiff system the motor velocity settled back to a constant level.

3.1.1 Experiment #1

We first measured motor speed for the cantilever beam system when the motor was driven at 0.75 volts. It varied as a function of beam stiffness, starting at 250 N/m (short span) and ending at 12,000 N/m. The motor velocity followed the same pattern for the simulation and the experimental data, **Figure 22**. Firstly, the motor velocity remains more or less constant, with little variations, until it reaches 1500 N/m where it suddenly drops to a lowest speed found at 3000 N/m. The motor velocity at this point is approximately 3000 rpm for the simulation and 2800 rpm for the experiment. Past this point it gently goes up. **Figure 23** shows the speed of the motor versus time for different beam stiffnesses, starting from a zero velocity. As can be seen

again, the final speed depends on the beam stiffness. The system settles quite fast given that the off-balance load is light.

Figure 24 shows the displacement of the beam as function of the velocity of the motor, normalized by the natural frequency of the system, which was determined experimentally as well and calculated for each beam stiffness. The key observation here is that the beam vibrates with the largest amplitude when motor velocity is near the resonant frequency of the system. **Figure 25** shows the vibration amplitude versus time for each beam stiffness.

Figure 26 shows how the motor velocity depends on the natural frequency of the beam. Note that when motor velocity is around 325 rad/sec, it happens to most closely match the natural frequency of the beam. As shown above (**Figure 24**), this creates a large amplitude vibration which then loads the motor, causing it to slow down.

Figure 27 shows the inertial loading on the motor as a function of beam stiffness. This plot confirms our hypothesis there is an optimal impedance that creates a high inertial load. A key finding that we did not anticipate was the decrease in inertial loading for very low stiffnesses. In retrospect, this makes sense in terms of considering the system as resonating beam. **Figure 28** shows the measured acceleration of the beam as a function of time for each level of beam stiffness.

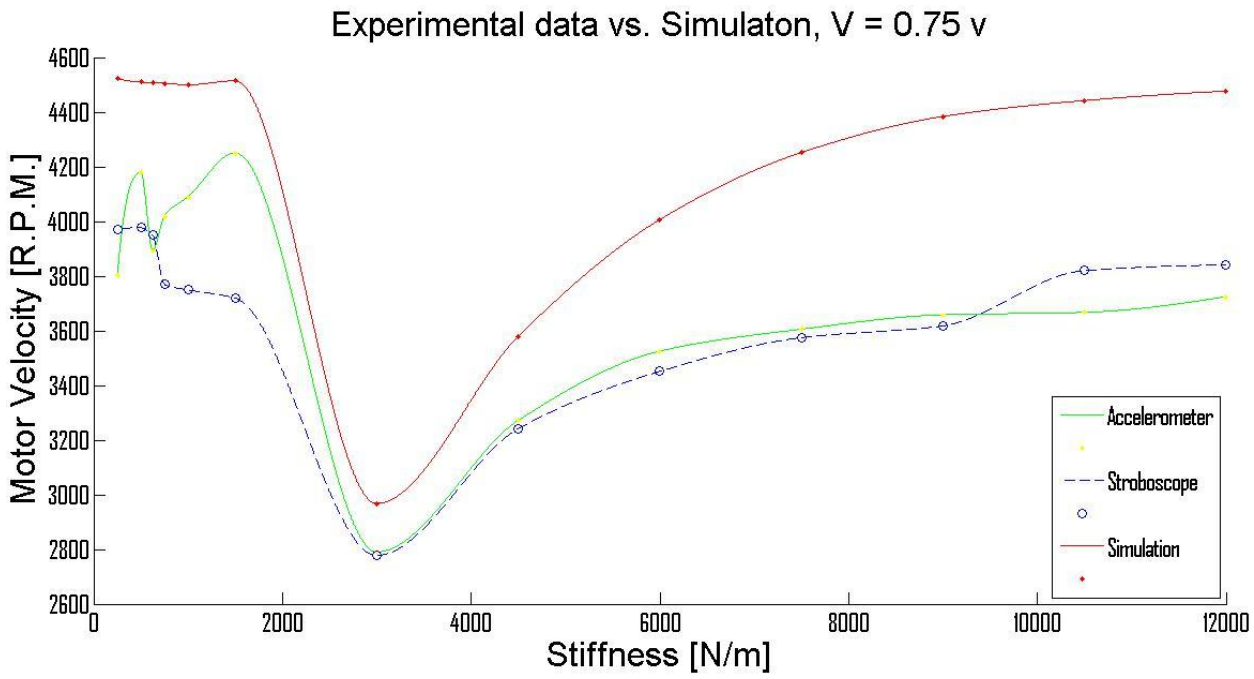

Figure 22: Experiment #1. Plot showing the comparison between simulation and data recorded by the accelerometer and stroboscope for stiffness levels [N/m]: 250, 500, 625, 750, 1000, 1500, 3000, 4500, 6000, 7500, 9000, 10,000 and 12,000.

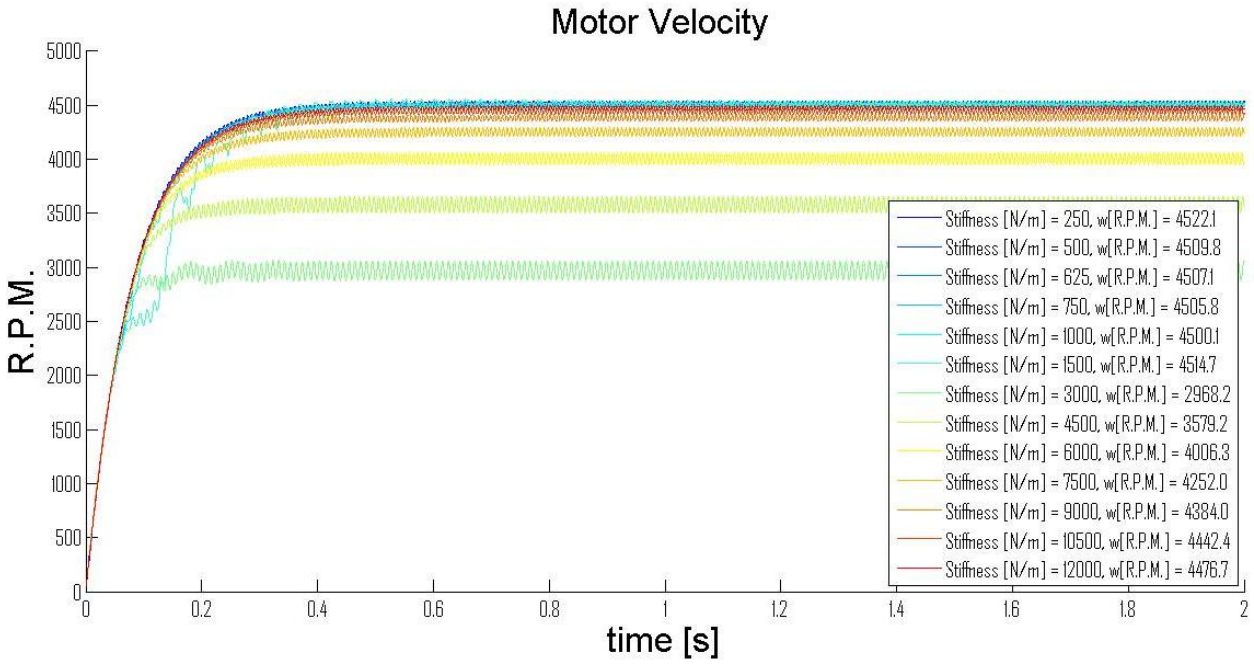

Figure 23: Experiment #1. Plot showing the evolution of motor velocity over time for the simulation.

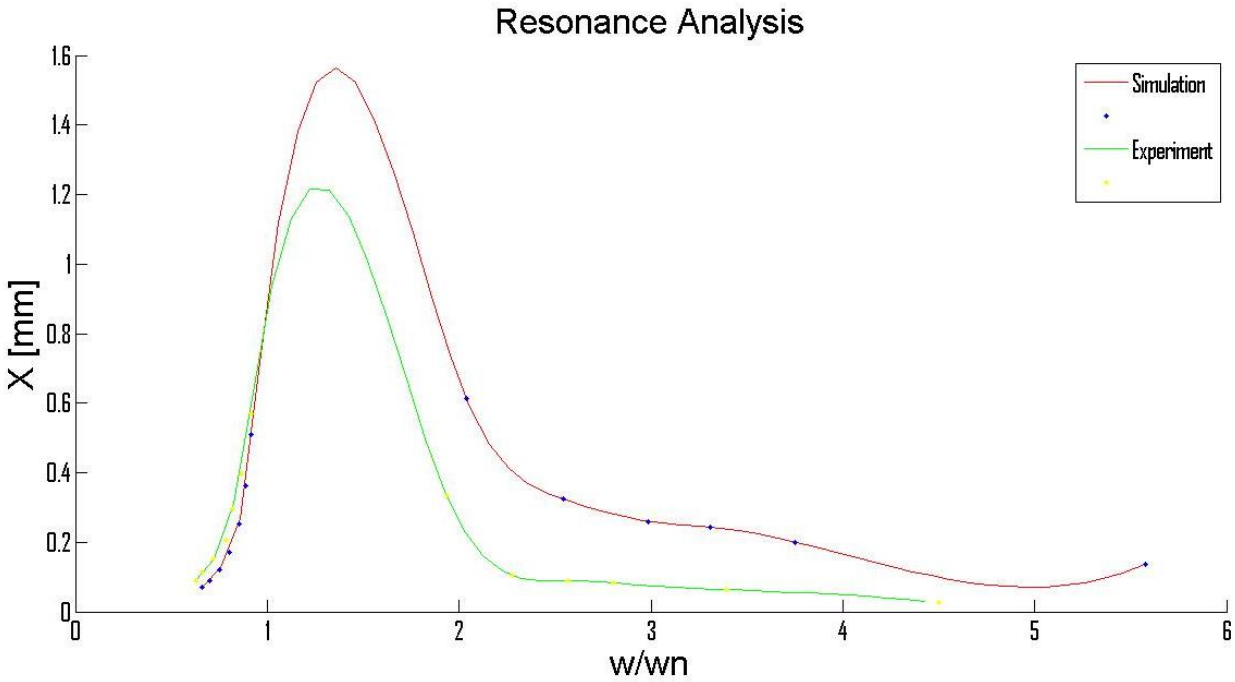

Figure 24: Experiment #1. Plot showing the resonance analysis for experiment #1. Simulation vs. Experiment results.

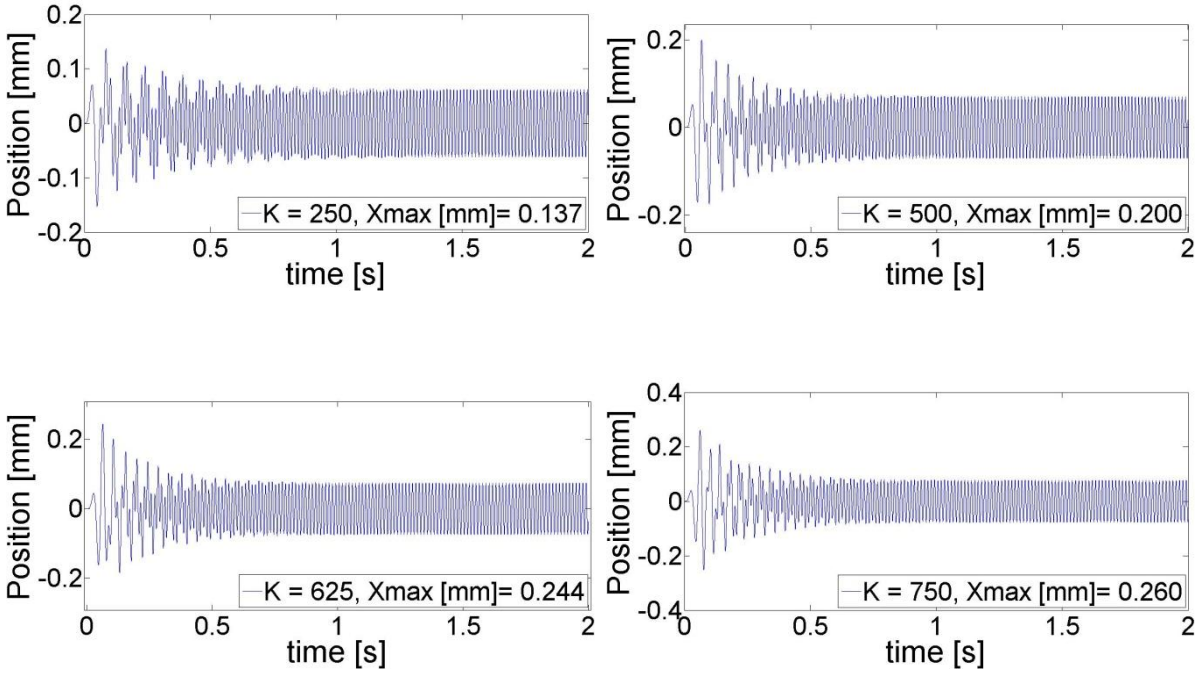

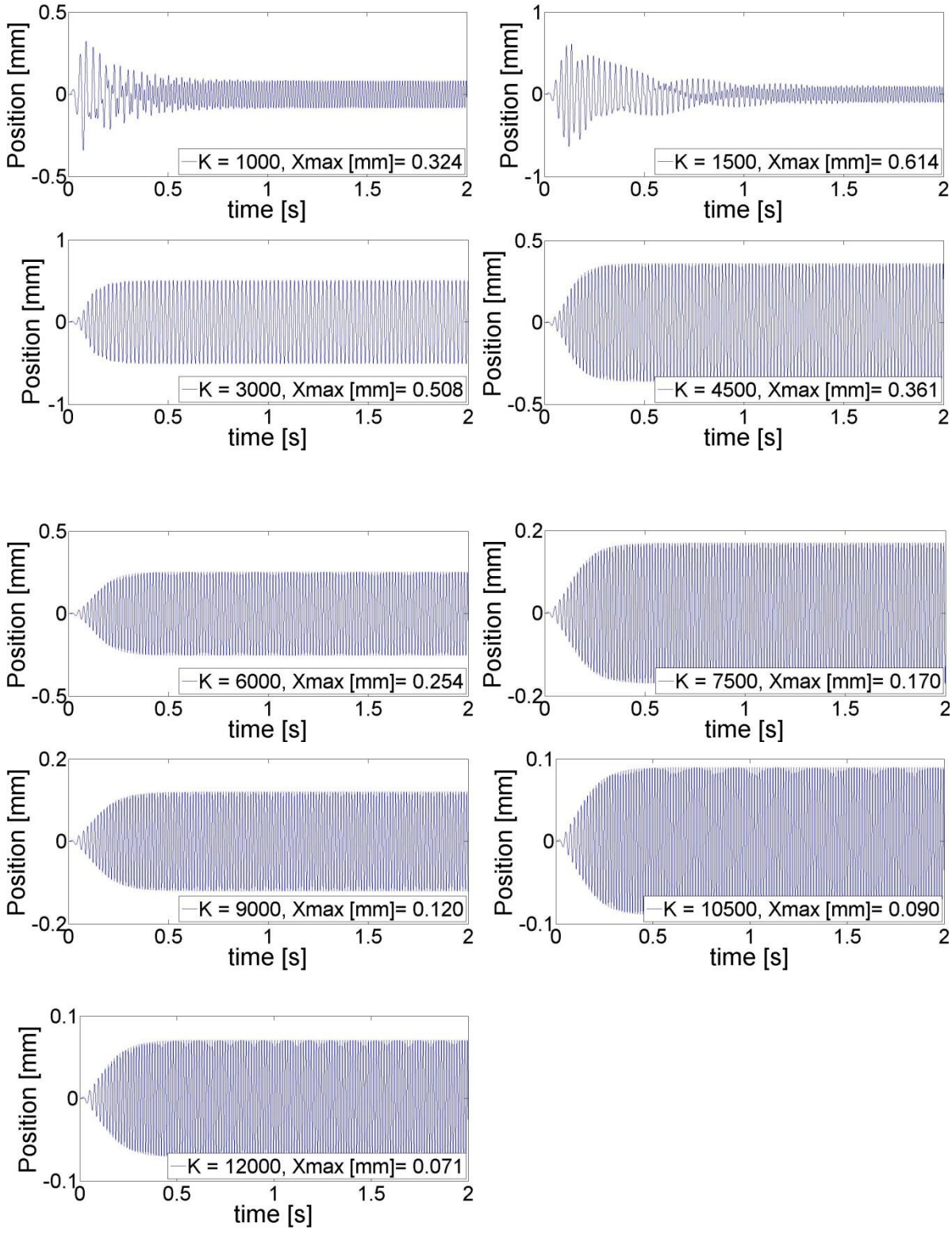

Figure 25: Experiment #1. Plots of vibration displacement for every stiffness, max amplitude at steady state taken in order to build **Figure 24**.

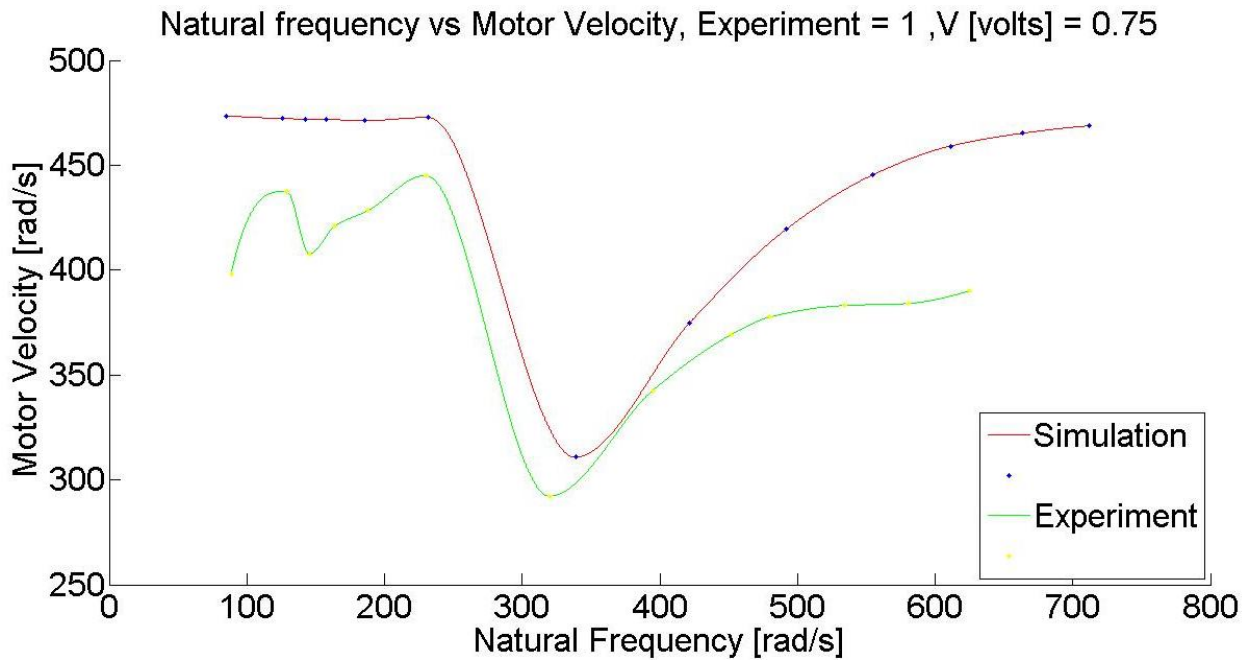

Figure 26: Experiment #1. Plot showing the natural frequency of the system for each stiffness vs. the motor velocity. When they match up the system is resonating.

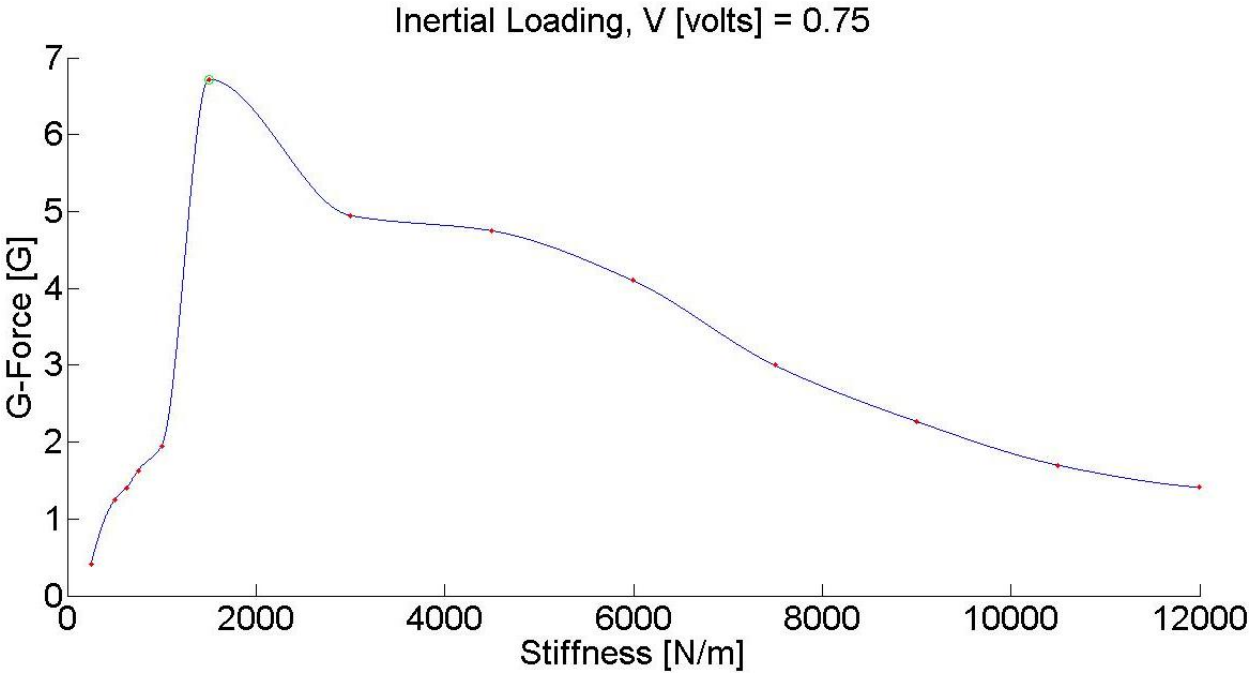

Figure 27: Experiment #1. Plot showing the vibration acceleration as a function of stiffness. System resonating for a stiffness of 1500 N/m.

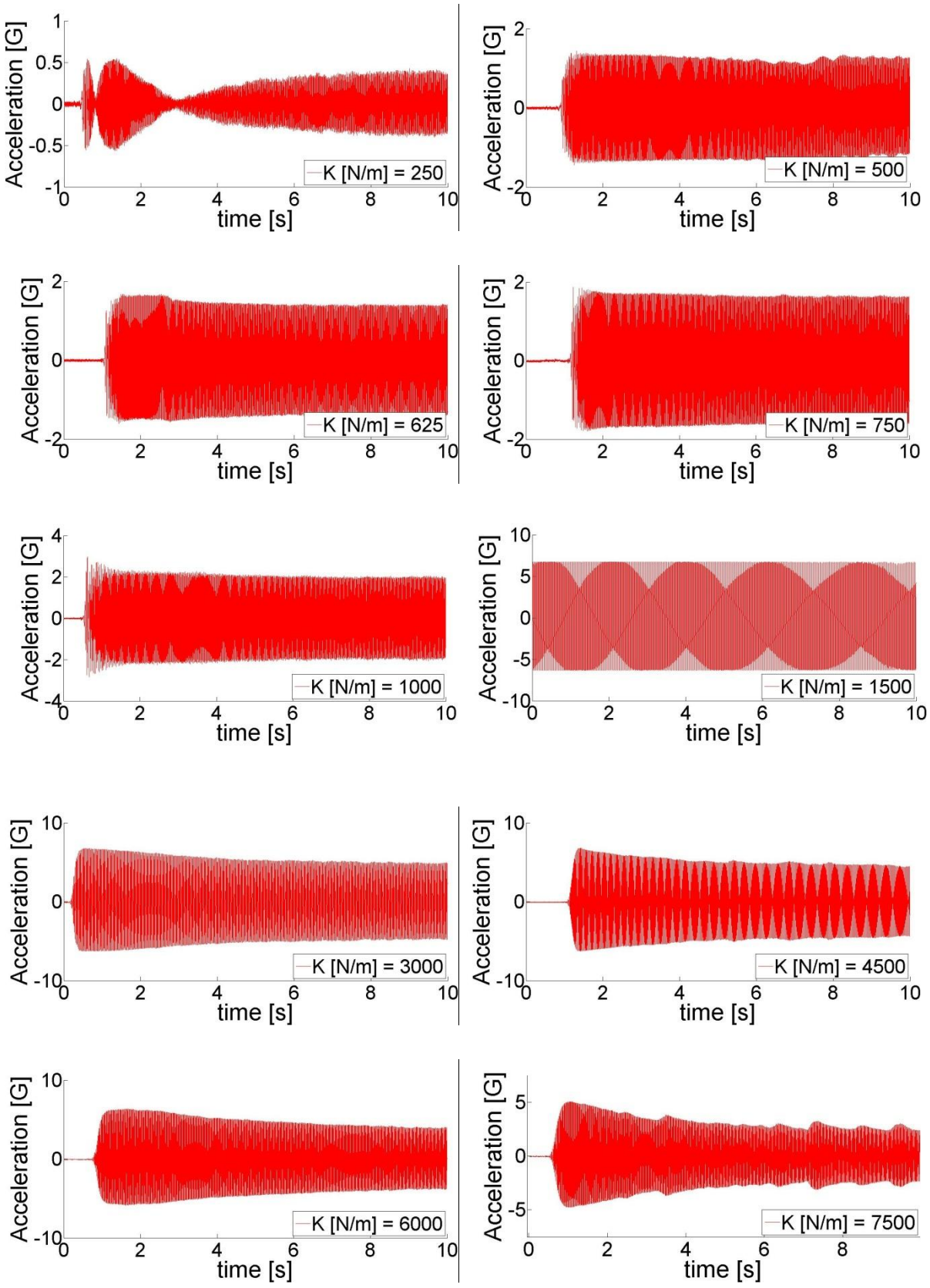
Acceleration [G]
time [s]
K [N/m] = 250
K [N/m] = 500
K [N/m] = 625
K [N/m] = 750
K [N/m] = 1000
K [N/m] = 1500
K [N/m] = 3000
K [N/m] = 4500
K [N/m] = 6000
K [N/m] = 7500

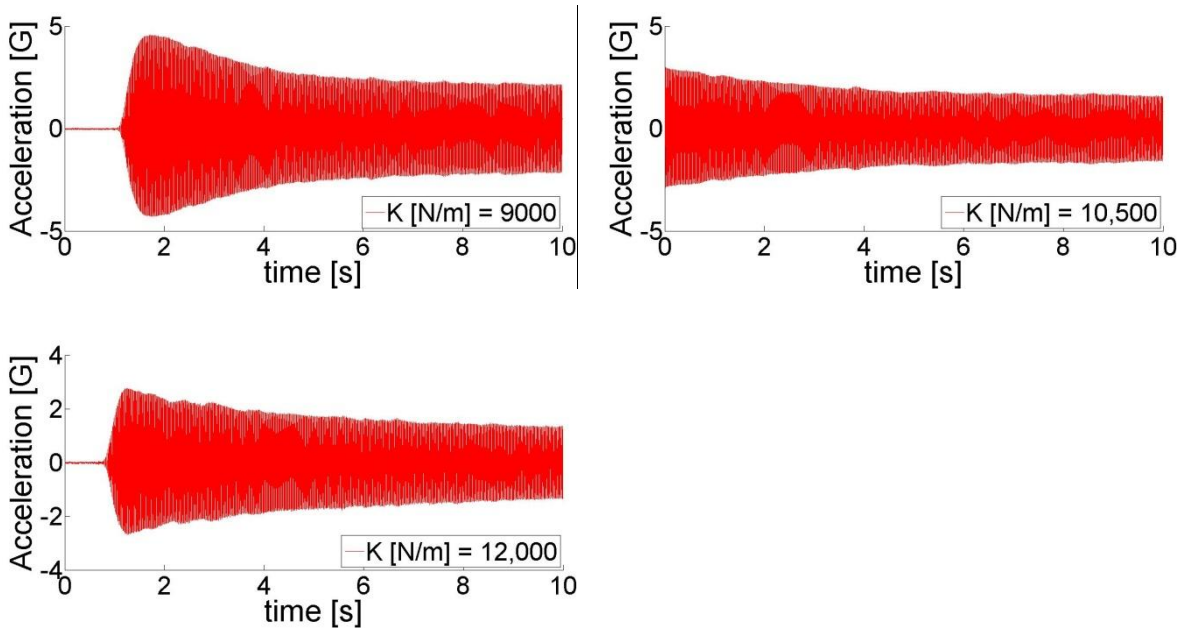

Figure 28: Experiment #1. Acceleration profile for every stiffness in g-force (9.81 m/s^2). Data used to build **Figure 27**. Plot for K = 1500 N/m, the accelerometer was saturated (acceleration > 6G) since the system is resonating.

3.1.2 Experiments #2 & #3

Figure 29-34 replicate the above results for motor input voltages equal to 1.5 volts and 2 volts, respectively. For these simulations and experiments, we also altered the off-balance load, using a larger load for the 1.5 volt condition, and a smaller load for the 2.0 volt condition. As can be seen, the motor speed again depends on the beam stiffness, and the simulation adequately captures this phenomenon.

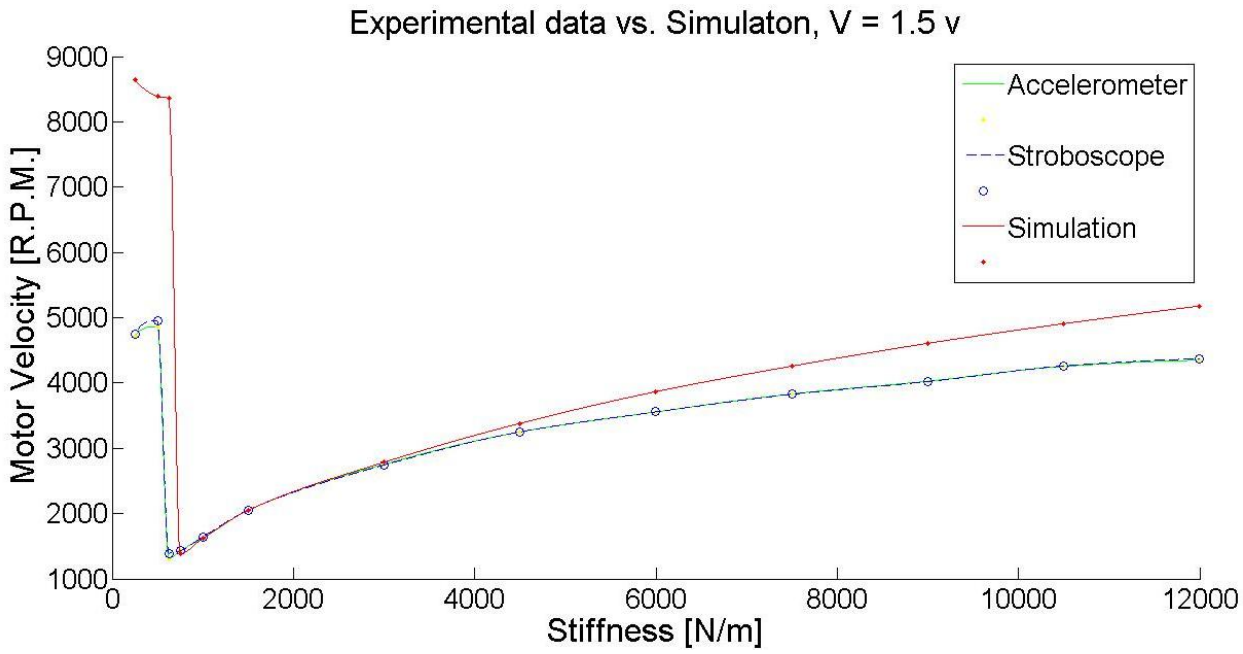

Figure 29: Experiment #**2**. Plot showing the comparison between simulation and data recorded by the accelerometer and stroboscope for stiffness levels [N/m]: 250, 500, 625, 750, 1000, 1500, 3000, 4500, 6000, 7500, 9000, 10,000 and 12,000.

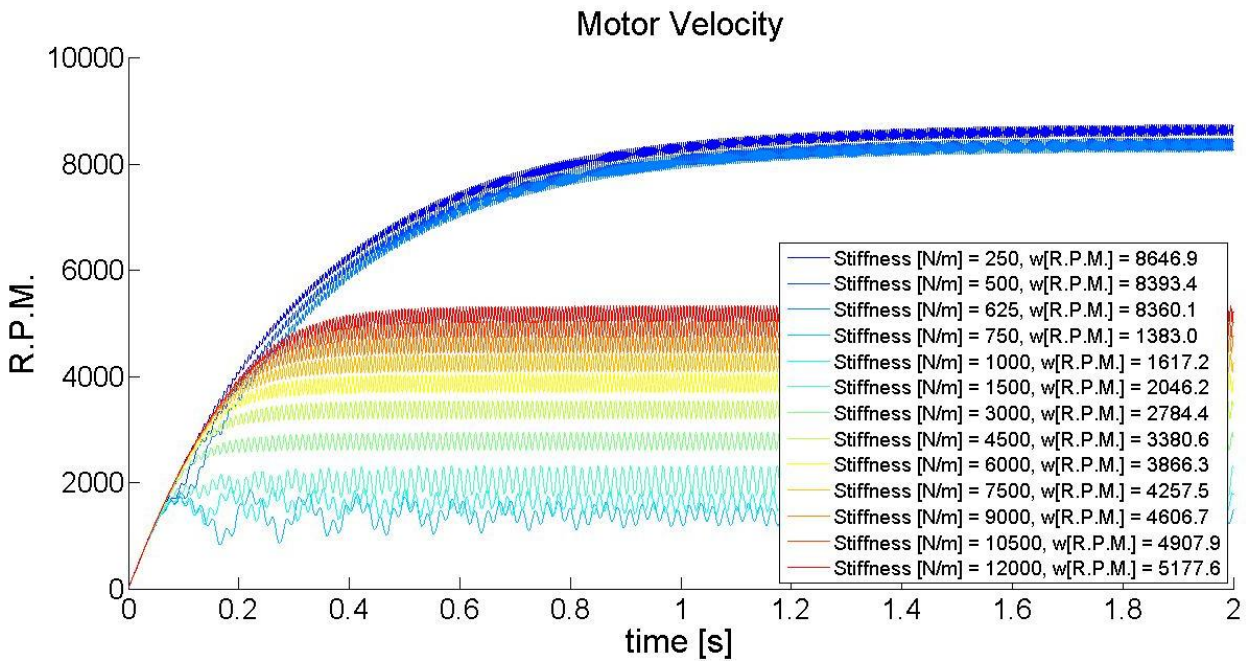

Figure 30: Experiment #**2**. Plot showing the evolution of motor velocity over time for the simulation.

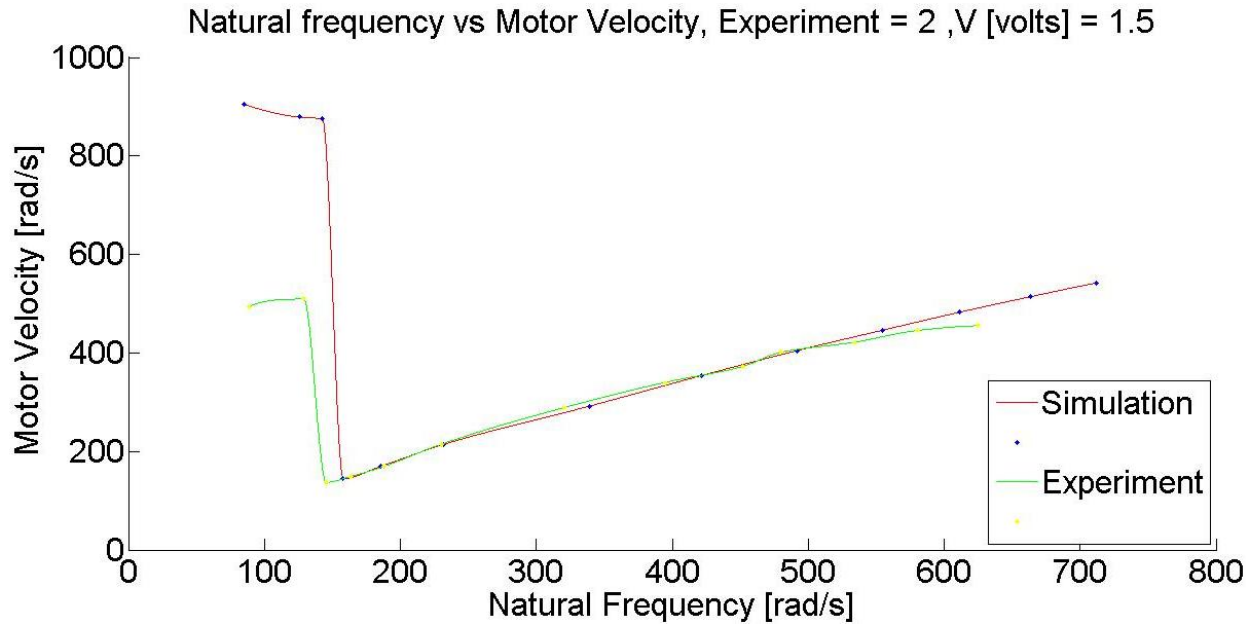

Figure 31: Experiment #**2**. Plot showing the natural frequency of the system for each stiffness vs. the motor velocity. When they match up the system is called to be in resonance.

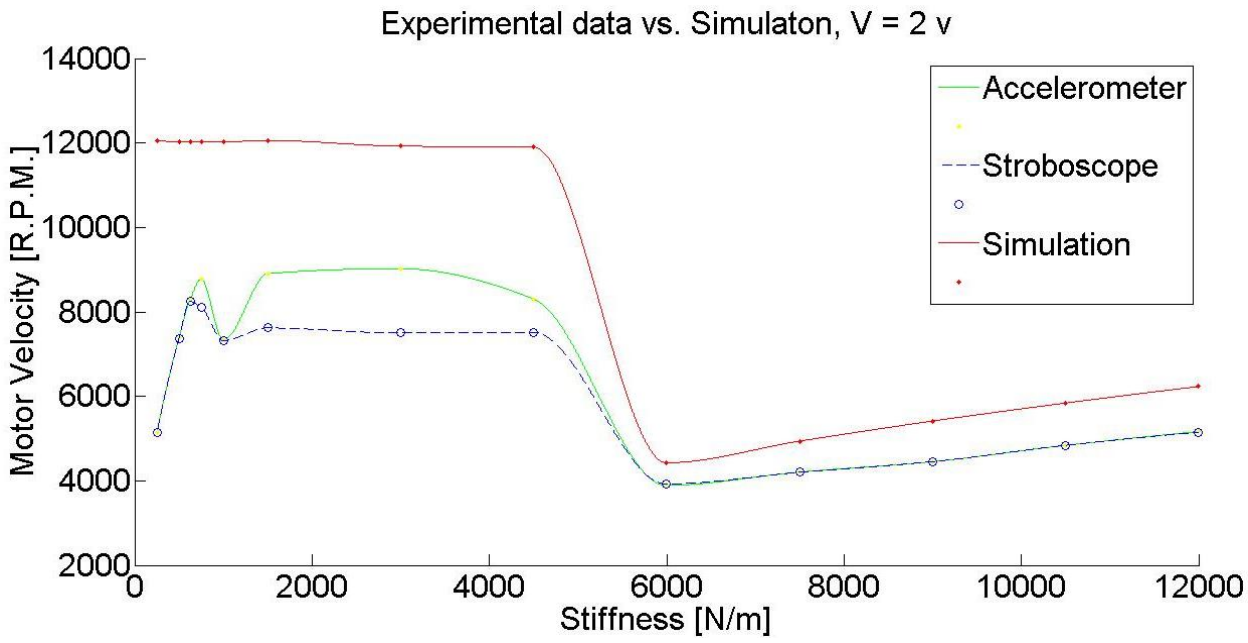

Figure 32: Experiment #**3**. Plot showing the comparison between simulation and data recorded by the accelerometer and stroboscope for stiffness levels [N/m]: 250, 500, 625, 750, 1000, 1500, 3000, 4500, 6000, 7500, 9000, 10,000 and 12,000.

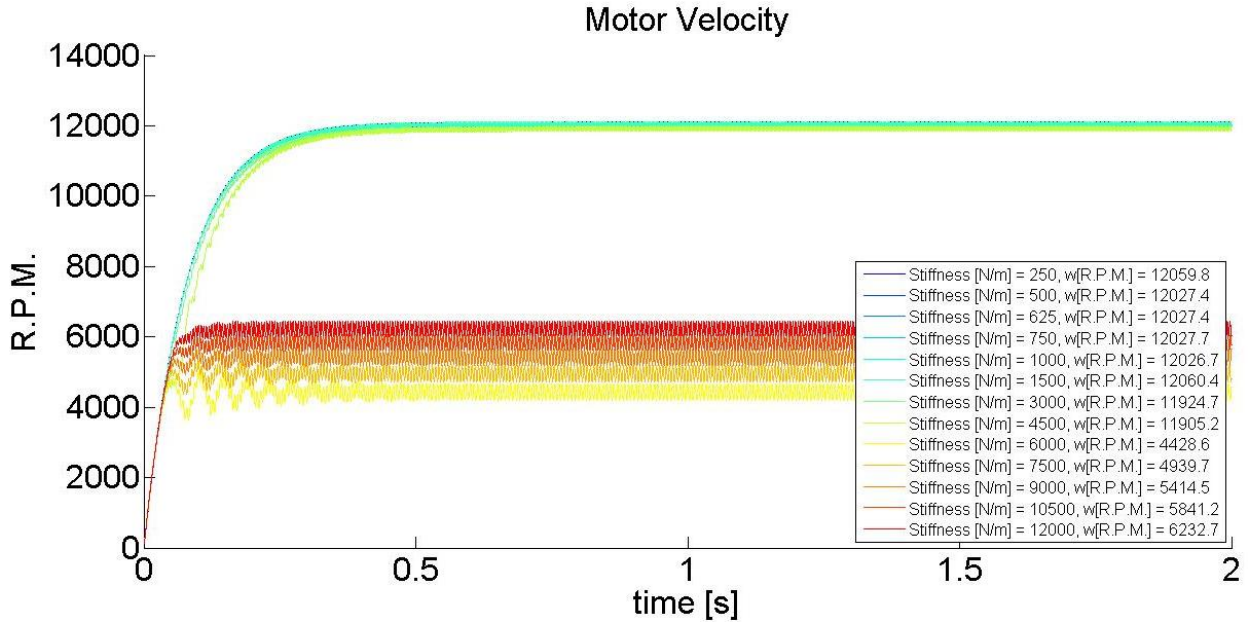

Figure 33: Experiment #**3**. Plot showing the evolution of motor velocity over time for the simulation.

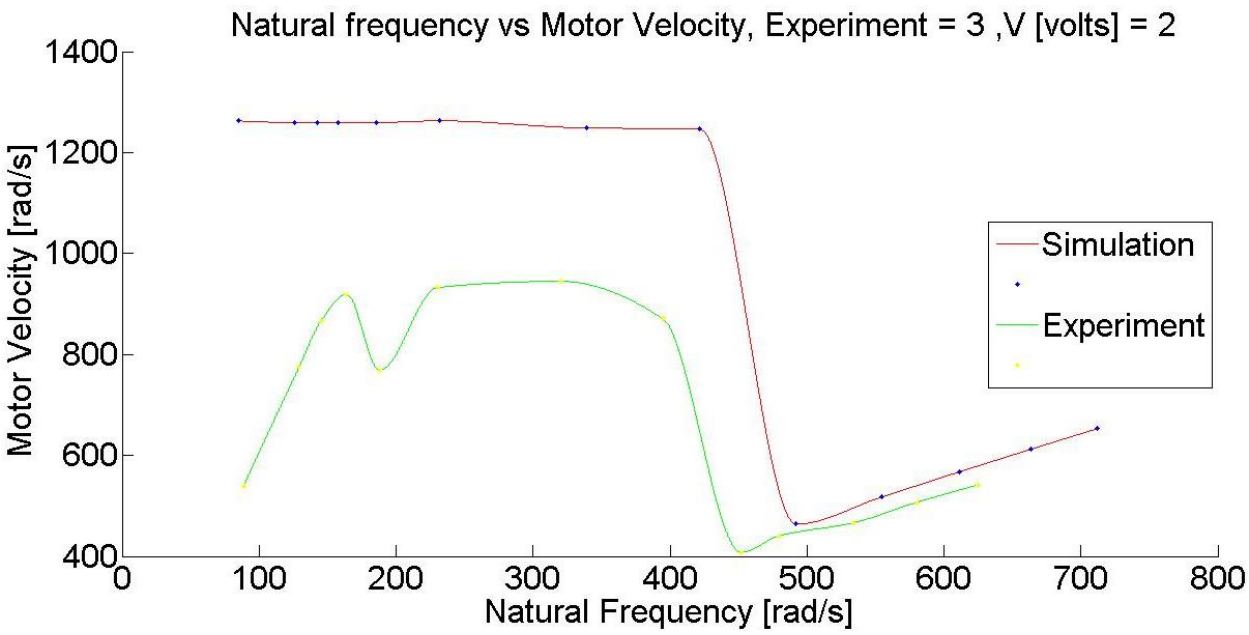

Figure 34: Experiment #**3**. Plot showing the natural frequency of the system for each stiffness vs. the motor velocity. When they match up the system is called to be in resonance.

3.1.3 Sensitivity Analysis

Given the confidence gained in the simulation by comparing the above experimental results with the simulation, we proceeded to examine how different system parameters affect the system behavior using simulation. **Figure 35** shows how the input voltage affects motor velocity as a function of beam stiffness. As can be seen, the stiffness at which motor velocity is slowest (i.e. where it is resonating the most), moves to the right as the driving voltage increases.

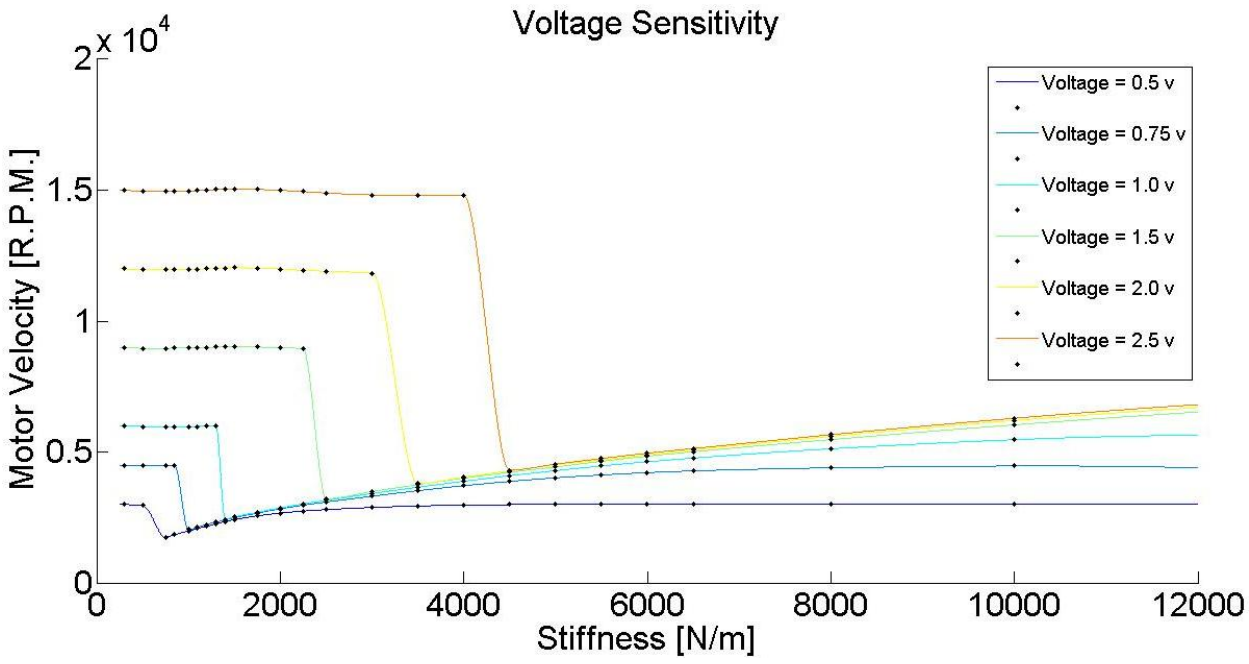

Figure 35: Plot showing the voltage analysis of sensitivity.

Figure 36 shows how motor velocity depends on the off-balance load as a function of beam stiffness. Increasing the off-balance load pushes the minimum speed point of the motor to a smaller stiffness.

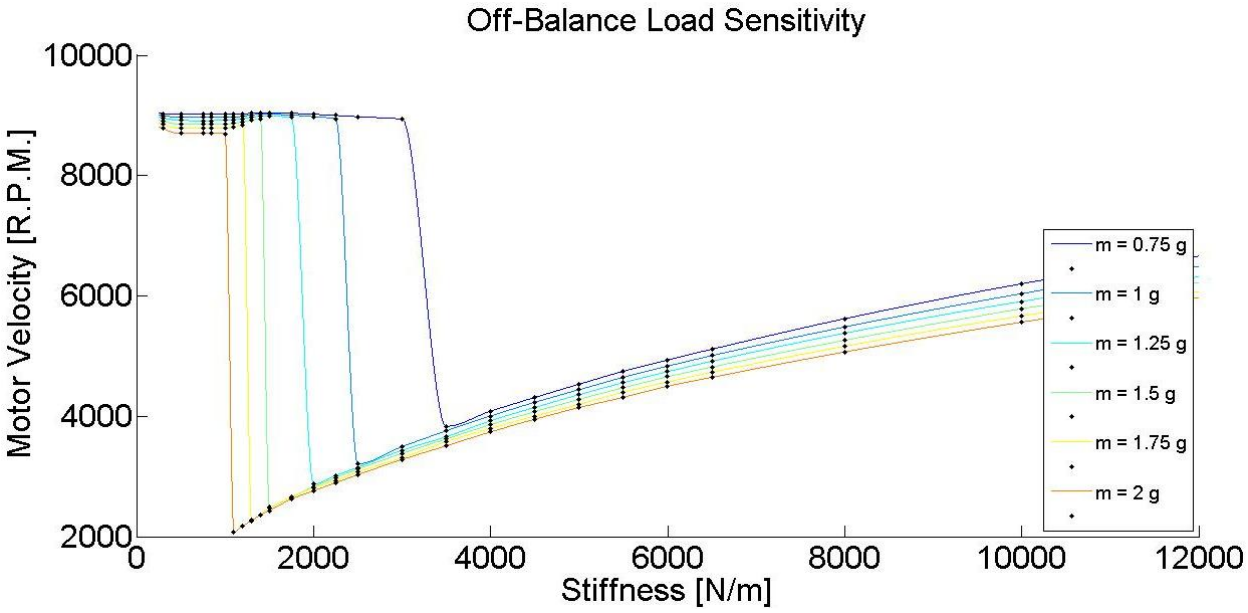

Figure 36: Plot showing the off-balance load analysis of sensitivity.

Figure 37 shows what happens when the system mass (i.e. mass of the beam, and in the actual ring sensor, 2.3.3**,** motor housing) are varied. Note that increasing the system mass moves the point of slowest velocity to the right. This is an important consideration as we will see for the ring sensor, as we desired the phenomenon of increasing speed with increasing stiffness to happen in a region consistent with human hand stiffness (i.e. the stiffness of the skin and muscle together), which reaches up to only 5016 N/m.

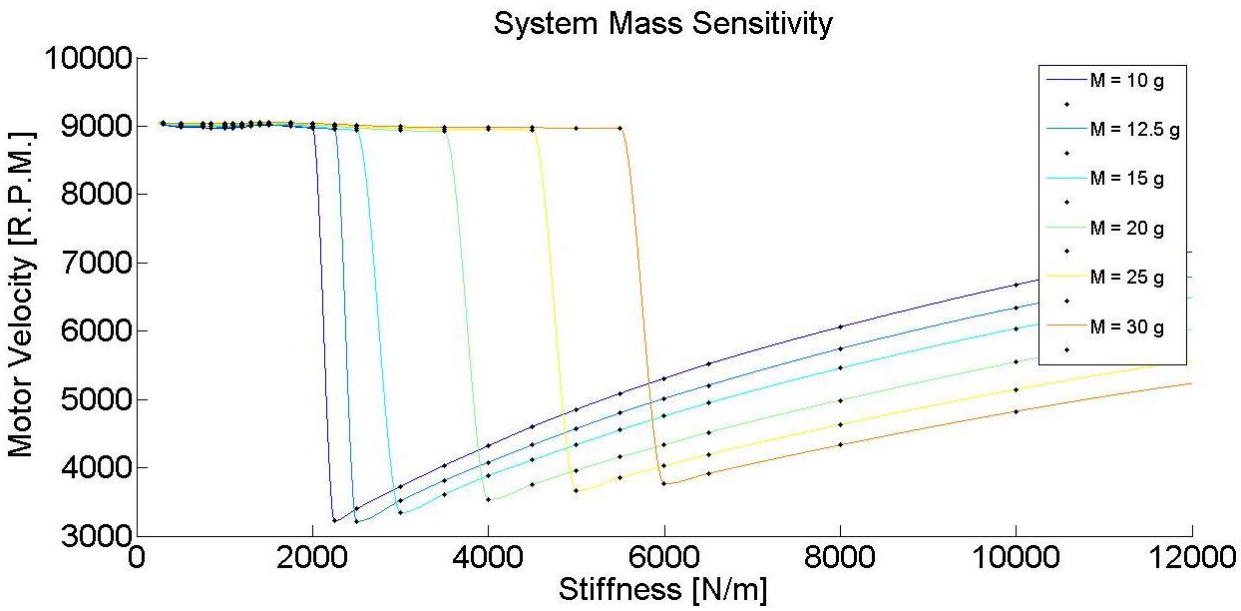

Figure 37: Plot showing the system mass analysis of sensitivity.

Figure 38 shows motor velocity at constant levels of stiffness as a function of motor input voltage. For an unloaded DC brushed motor, we expect the motor velocity to increase linearly with motor input voltage. This is true for the system at low and high input voltages, which drive the system at frequencies far away from the beam resonant frequency. However, for input voltages that cause motor velocities near the beam resonant frequency, the beam vibrates a lot, loading the motor, and slowing it down.

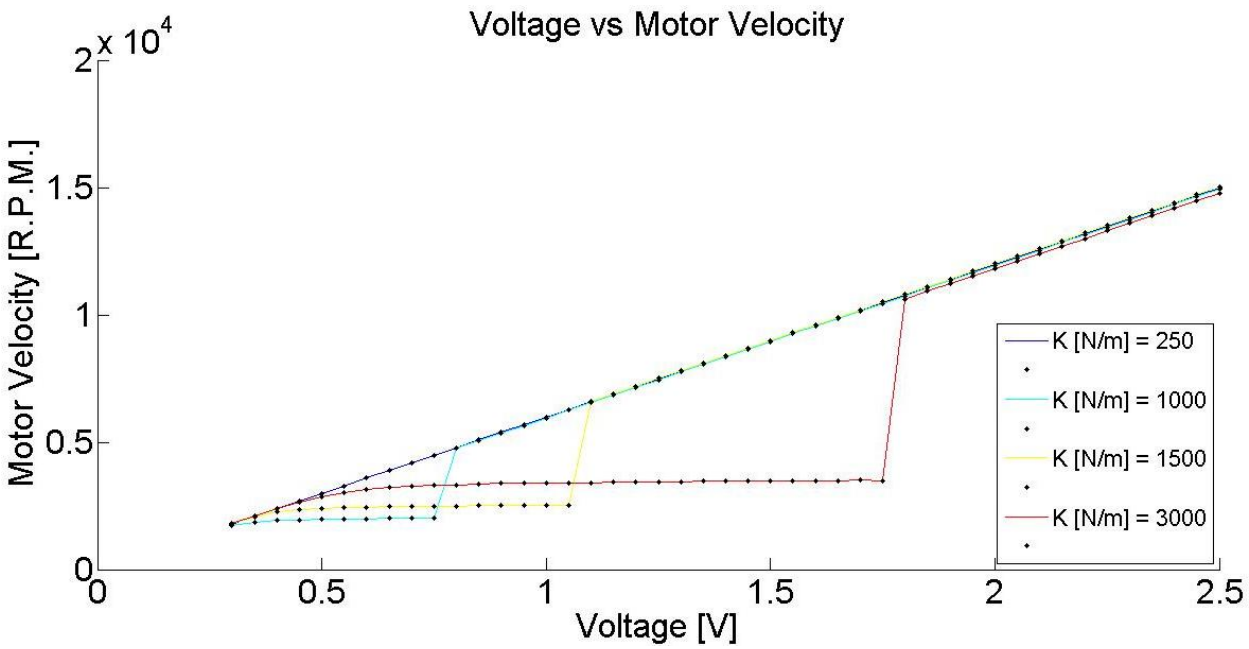

Figure 38: Plot showing the evolution of motor velocity as we vary the voltage for constant levels of stiffness.

3.2 Ring Sensor Experiment

In this experiment, a force transducer handgrip (2.3.1.4) was squeezed with a progressive level of force, from zero to one hundred NFL (Normalized Force Level in %), with corresponding levels of total stiffness of 25 - 5016 N/m, and damping of 1 - 17 N-s/m **(**2.2.1 and 2.2.2). Acceleration and grip force were recorded for ten seconds, We found that at the very beginning as we touched the handgrip the motor rotated at a high speed, and that the speed decreased to a low value as we reached motor velocities near the natural frequency. It was followed by a linear increase in frequency (motor velocity) and decrease in acceleration (inertial load) for experiment #1 (smaller off-balance load), and nearly linear for experiment #2 (larger off-balance load).

Hence, both experiments confirmed our hypothesis that grip force and muscle stiffness vary with motor velocity. Note that the simulation was done taking into account total stiffness, however for the plots **Figure 41** and **Figure 44**, only muscles stiffness was plotted vs. frequency, subtracting K_{Skin} from K_{Total}.

Force levels were within the normal range of grip force when squeezing a cylinder [5], [6], which was a good indicator, with a maximum of 4.5 N for the first experiment (**Figure 39**) and 6 N for the second one (**Figure 42**).

In both experiments #1 and #2 simulation and experimental data follow each other, meaning that we achieved a good model of the ring sensor and the estimation of the parameters was good.

Finally, both relationships stiffness vs. frequency and NFL vs. frequency, follow the same patterns (high frequencies first for low values, a minimum when the motor velocity is near the

natural frequency of the system and followed by a smooth increase of frequency again), which shows that muscle stiffness and muscle force are strictly correlated.

3.2.1 Experiment #1

Figure 39 shows a smooth decrease in acceleration as the grip force increases (from 2 sec to 4.5 sec), going to a lowest acceleration when the grip force is maximum. Then, as we started to relax our hand (around 6.8 sec) and the grip fore dropped, it accelerates again. The same phenomenon happens with grip force and frequency, which is more discernible in **Figure 40**. When grip force increases the frequency is higher and vice versa.

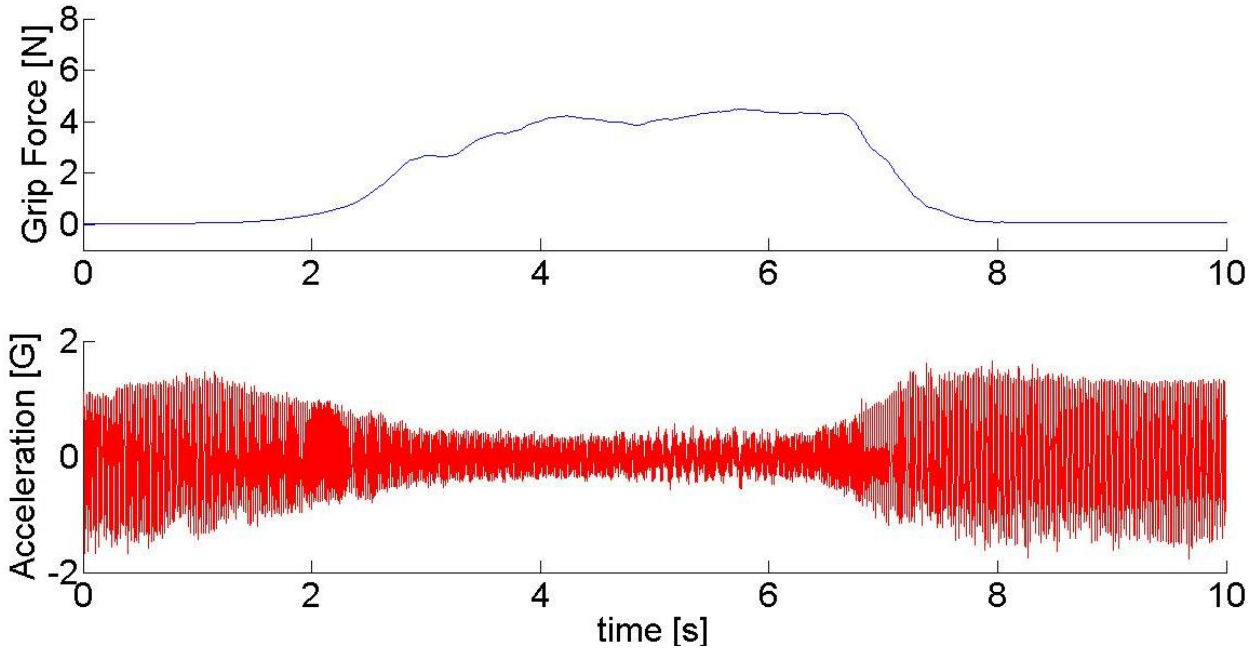

Figure 39: Experiment #1. Force transducer grip force measurements and accelerometer data profile.

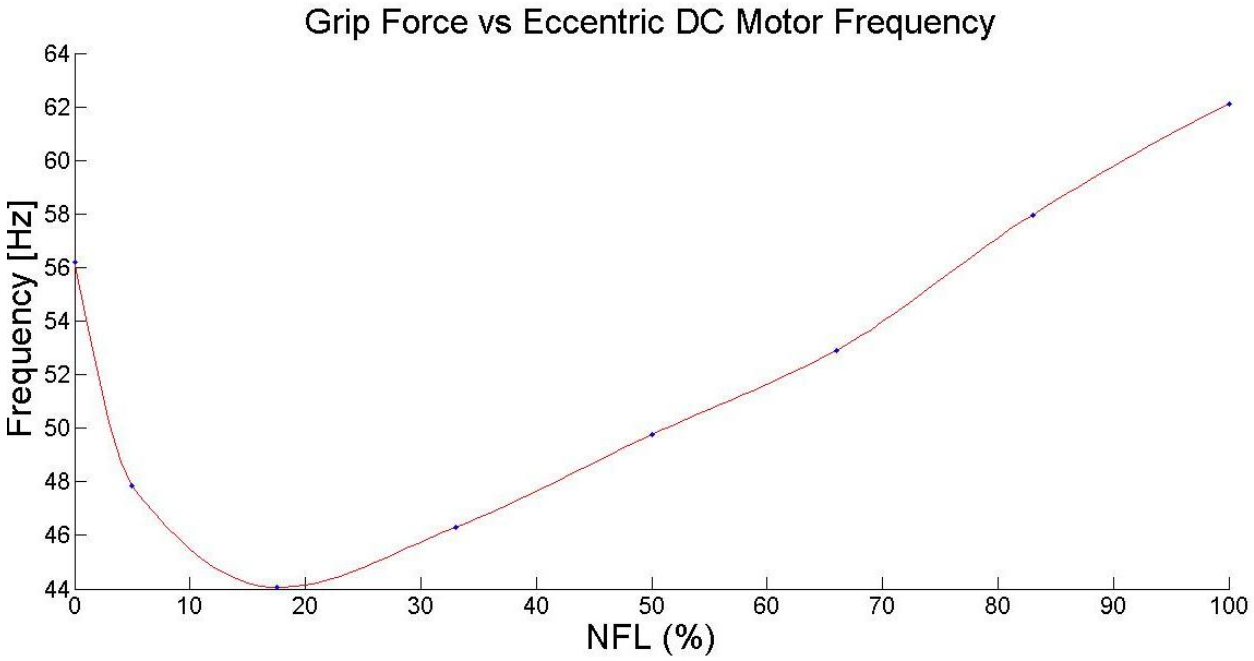

Figure 40: Experiment #1. Normalized force level versus motor frequency. Data from **Figure 39**.

Figure 41 shows the same pattern for simulation and experimental data, however, there is a little offset between both curves.

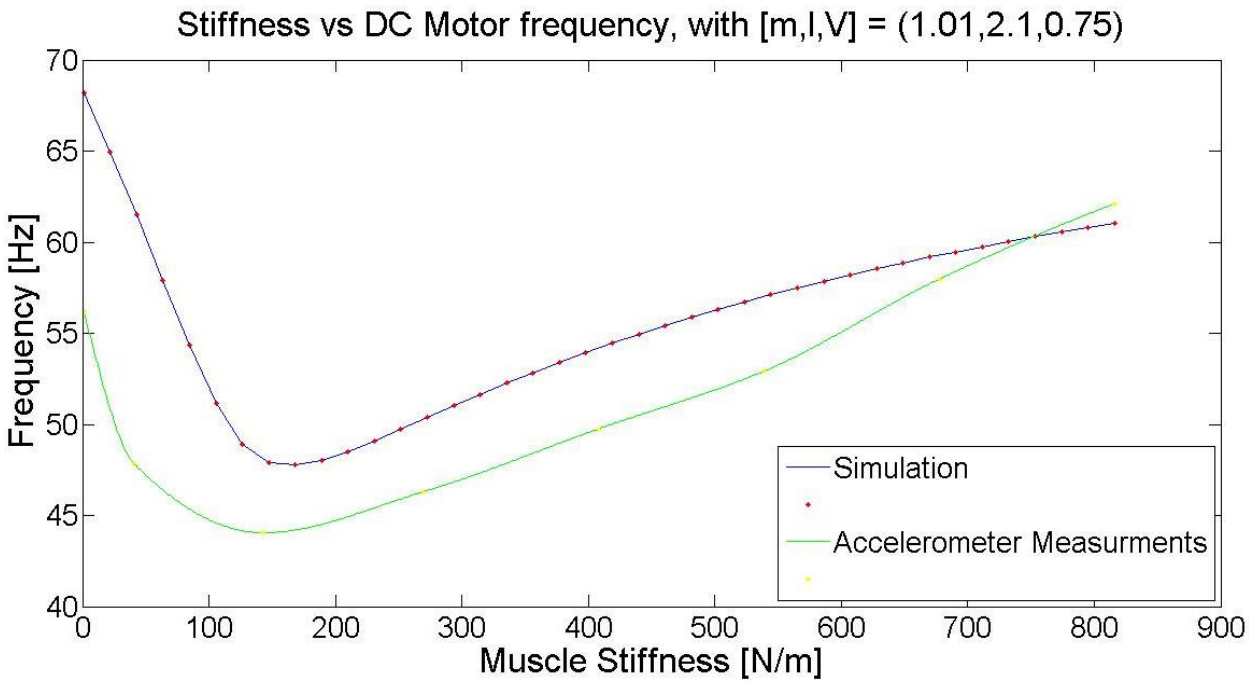

Figure 41: Experiment #1. Comparison between simulation and experiment. Muscle stiffness is related to NFL (%) through **Figure 5**.

3.2.2 Experiment #2

Experiment #2 replicates Experiment #1 with larger forces and accelerations (**Figure 42**) since it was carried out with a larger off-balance load. However, lower motor frequencies (**Figure 43** and **Figure 44**).

As can be seen, the motor speed again depends on the stiffness, and the simulation again adequately captures this phenomenon.

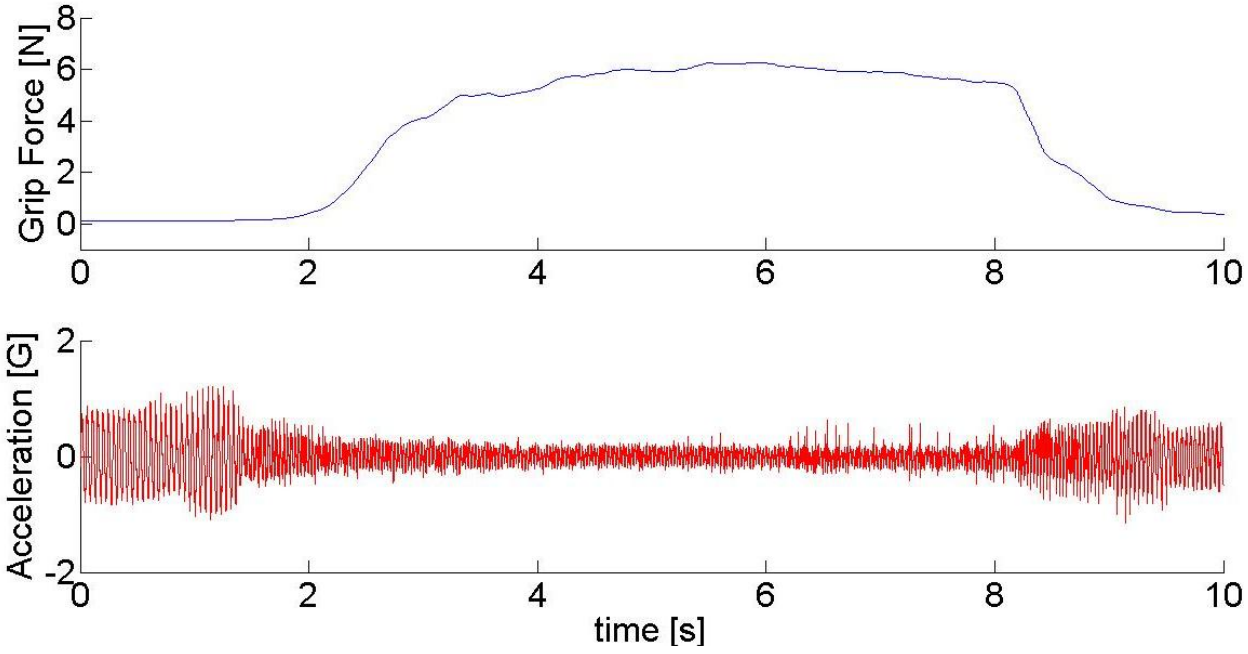

Figure 42: Experiment #2. Force transducer grip force measurements and accelerometer data profile.

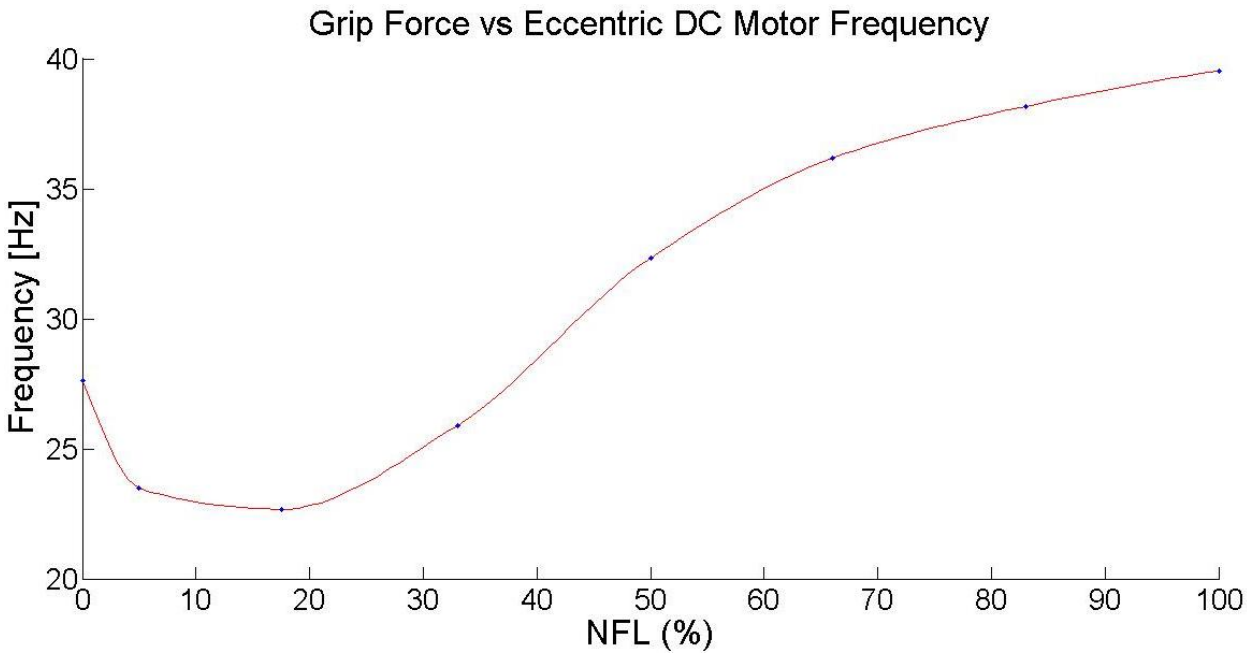

Figure 43: Experiment #2. Normalized force level versus motor frequency. Data from **Figure 42**.

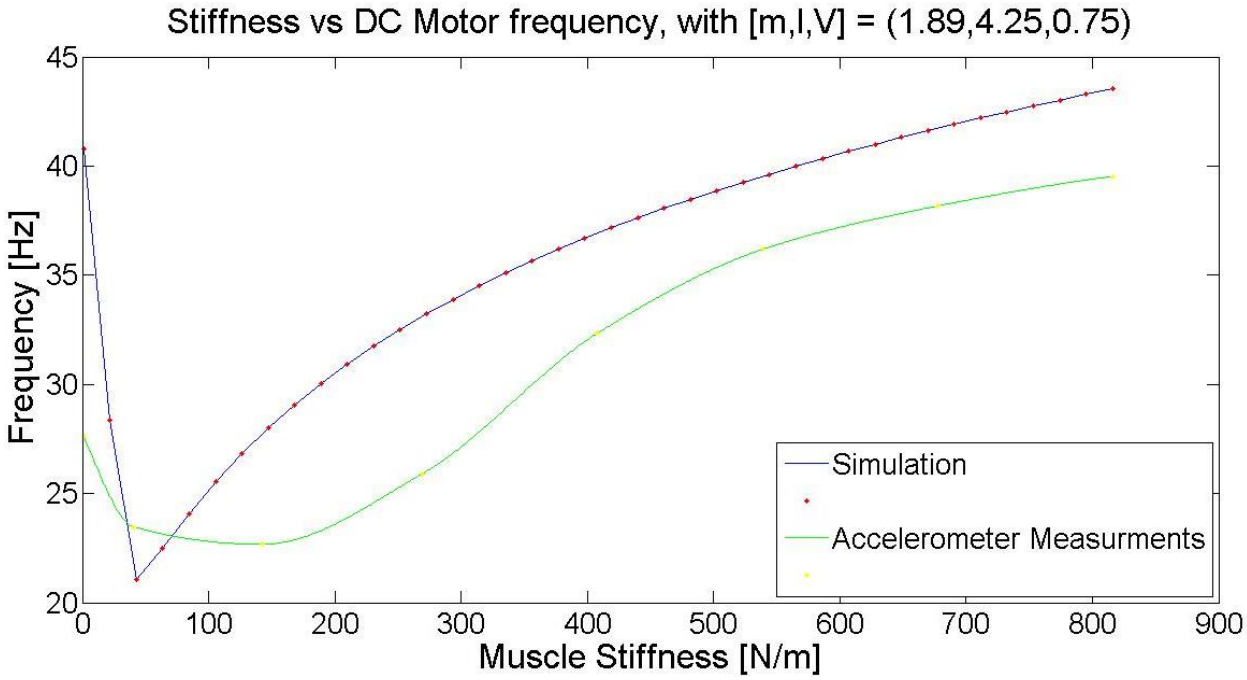

Figure 44: Experiment #2. Comparison between simulation and experiment. Muscle stiffness is related to NFL (%) through **Figure 5**.

Figure 44 shows the same pattern for simulation and experimental data, however, there is a little offset between both curves.

3.2.3 Optimization Routine

The simulation took 4h and 21 min. It was run using a computer with the following properties:

- Operating system: Windows 7.
- Processor: Inter(R) Core(TM) i5-2430M CPU @ 2.40GHz 2.40 GHz
- Installed RAM memory: 6.00 GB
- System type: 64-bit Operating System

Table 8: Optimal parameters.

Solution	OPTIMAL PARAMETERS
Voltage [volts]	**0.5**
Off-balance load [g]	**2**
Eccentricity [mm]	**2.5**

Figure 45 shows trade-off (**Eq. 21**), sensitivity and g-force vs. the combination index. **Figure 46** shows the combination of parameters per each index defined. The optimal solution is found at combination index **20**.

As can be seen, the optimal point did not happen to have neither maximum sensitivity nor lowest g-force, however it was the best trade-off between them. Also, an inertial factor of 12.5 $g \cdot mm^2$ (above the average) was the optimal, with the lowest level of voltage considered.

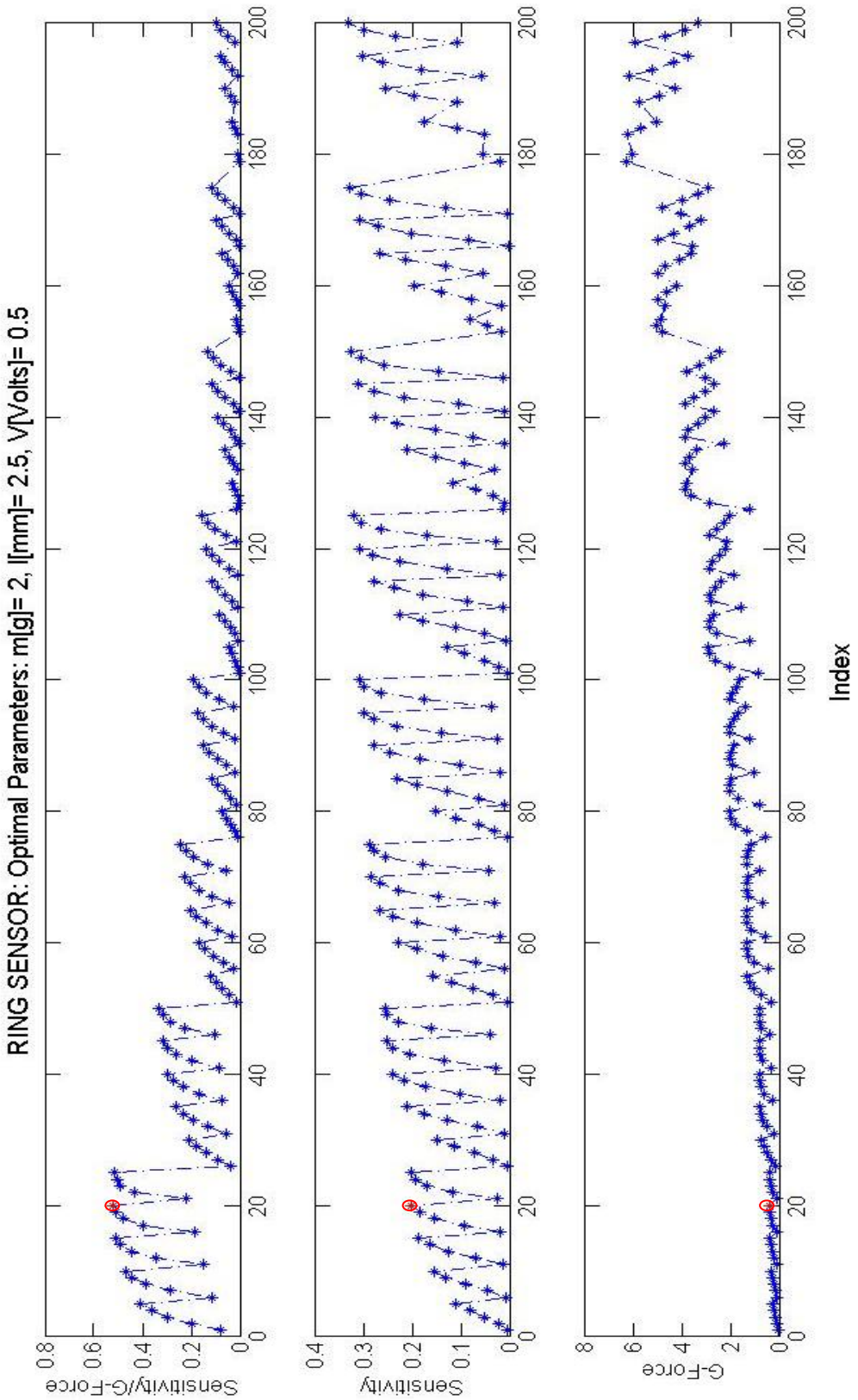

Figure 45: Plot showing the trade-off between ring sensor sensitivity and g-force, and the optimal point in red.

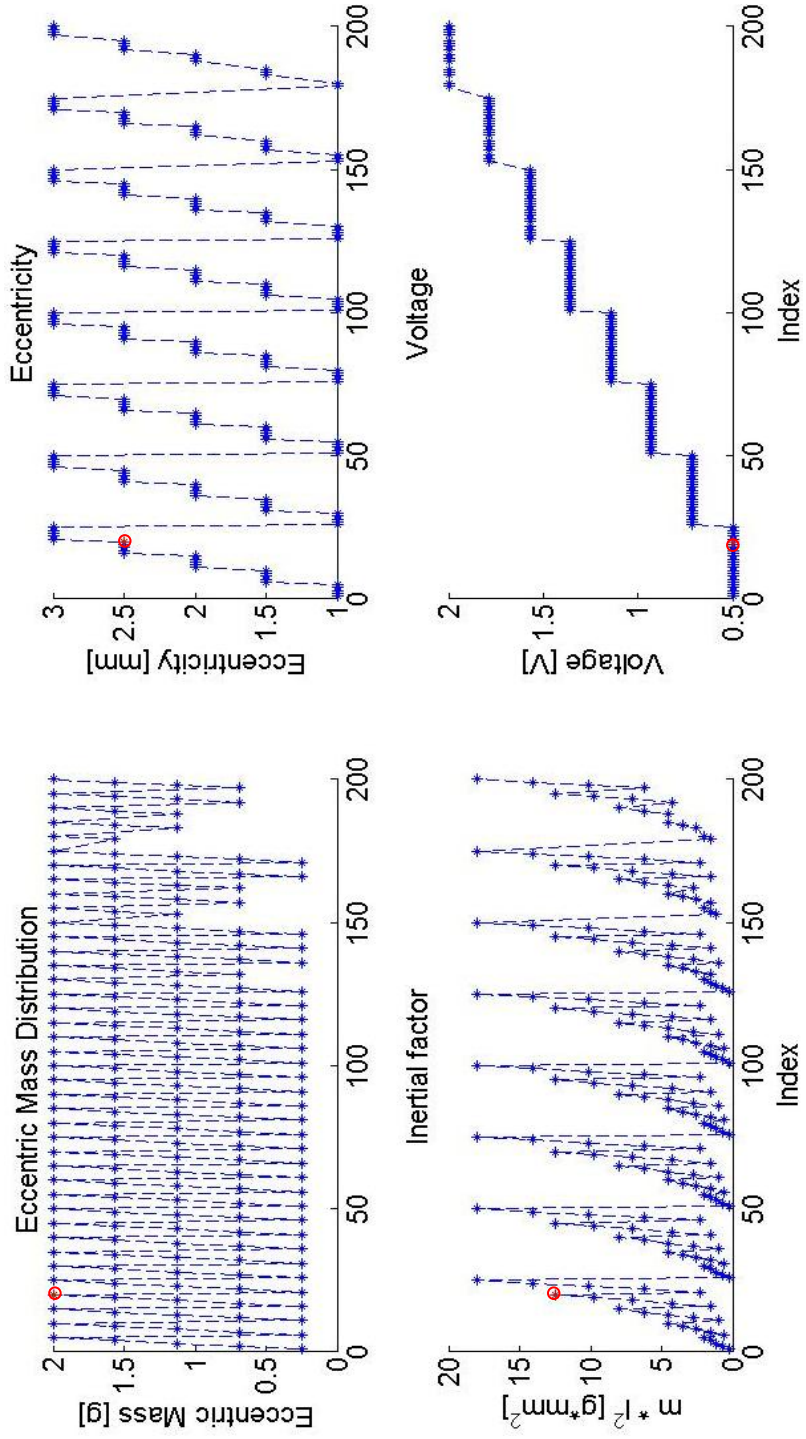

Figure 46: Optimal set of parameters, red point.

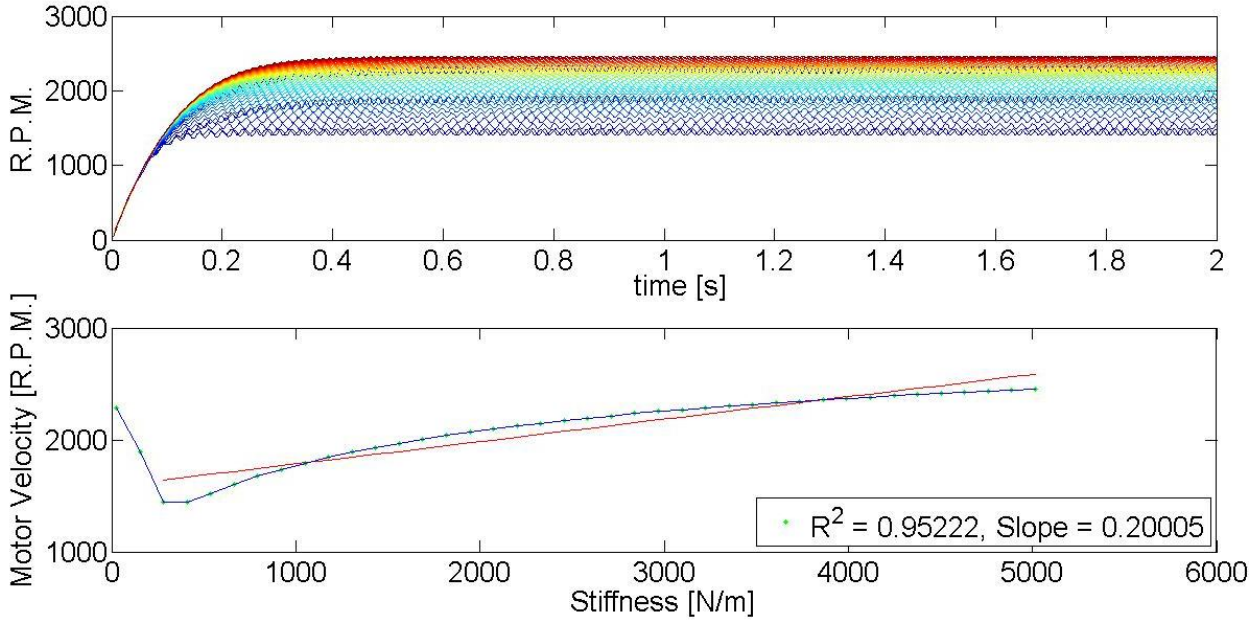

Figure 47: Optimal system behavior

Figure 47 shows the behavior of the system with the optimal set of parameters. The correlation coefficient 0.952 is smaller than 0.96 which indicates that the correlation between stiffness and motor velocity could not be accepted as linear. And for most stiffnesses it settles before 0.3 sec.

However, it is nearly linear and most importantly, the motor speed increases with stiffness which is the kind of behavior that we were interested in for our ring sensor.

Finally, if this ring sensor design were to be implemented, we can estimate the sensitivity. We assume human hand stiffness (K_{Skin} plus K_{Muscle}) variese in a range between 25 - 5016 N/m, and assuming that the initial stiffness given to the system sets the motor speed right before resonance (lowest point in **Figure 47**), i.e. 280 N/m. The motor would speed up from 1450 rpm. to 2455 rpm. for a level of 100 % of NFL applied. That is an increase of 1005 rpm, and assuming that the

highest grip force applied was 8 N, we would have a sensitivity of 125.6 rpm./N and a g-force (**Figure 45**) of 0.38-g.

4 Discussion

In this thesis, we studied how the velocity of an eccentric mass vibration motor driven at a constant voltage varies with the mechanical impedance of the system it is attached to, and specifically studied this phenomenon when the motor is worn as a ring sensor, to determine the feasibility of using the phenomenon to create a non-interposed grip force sensor.

We develop a dynamic model of the motor-skin interaction using Lagrange's equations. Motor velocity varies with grip force and muscle stiffness, as confirmed here both with the simulations of the model and with experiments. We found high motor velocities for very low levels of stiffness. Then, suddenly the inertial loading on the motor increases as the motor slows down to a minimum point near the natural frequency, defined by stiffness and system mass. This is followed by a near linear increase in motor velocity for medium levels of stiffness. Eventually, for a very stiff system the motor velocity settles back to a constant level. This pattern indicates that the interactions between motor speed, vibration, and hand impedance can be interpreted within a framework of resonance of the hand with the motor. When the motor rotates at a speed close to the resonant frequency of the hand, the system vibrates more, which applies an inertial load to the motor and slows it down. Put another way, the inertial loading effects on the motor (**Figure 27**) confirmed our hypothesis that for a lower impedance system the vibratory displacement is high, creating a greater inertial load on the motor. Since the motor is driven at a constant voltage, higher impedances cause the motor to speed up.

Some differences were found between simulation and experimental results. The pattern followed by the relationship between stiffness and motor velocity was the same in both cases. However, sometimes there was a little offset between both curves. This offset might be due to either a not accurate enough model for the dc motor or some small errors in the computation of parameters such as off-balance load and system mass.

The sensitivity analysis, **Figure 35**, **Figure 36** and **Figure 37**, tells us that the selection of a proper set of parameters is a key factor in order to achieve a steep effect for the ring sensor. We desired the phenomenon of increasing speed with increasing stiffness to happen in a region consistent with human hand stiffness, therefore a smaller voltage and system mass with a larger off-balance load, happen to be more appropriate parameters to consider. This is also supported by the optimization routine 3.2.3, where a low voltage is picked since high voltages generate a too high g-force (**Figure 45**), with a large off-balance load.

For the ring sensor grip force measurement, a much higher force was recorded in the second experiment with a larger off-balance load mounted (**Figure 42**), than in the first one with a smaller load. That could have been caused by either the ability of the subject to exert a larger squeezing force in the second experiment or the effect of the larger off-balance load. That suggests that an investigation on the off-balance loading effects vs. grip force should be carried out in order to determine whether the grip force measurement can be altered by the off-balance load mounted or not.

Figure 47 shows a quick settling time, smaller than 0.3 seconds for most levels of stiffness. This gives a sense of the bandwidth of the system, meaning how fast the dc motor can respond to a change in impedance. A fast response will enable the motor to react rapidly, producing a fast

change in speed. Hence, for the ring sensor experiment the bandwidth seems to be appropriate since motor speed changes very fairly rapidly with grip force, and human grip force is band limited to about 2 Hz.

Motor velocity was related to hand impedance under the assumption that skin impedance increased linearly and also assuming that muscle stiffness could be taken from [4]. However, in a further stage of this study other methods to obtain better measurements for hand stiffness could be considered, as for example [7].

Bibliography

[1] Bruce J. P. Mortimer, Gary A. Zets and Roger W. Cholewiak. "Vibrotactile transduction and transducers". *Enginnering Acoustics, J. Acoust. Soc. Am.*, vol. 121, pp: 2970-2977, 2007.

[2] Ronnie Lundstrom. "Local Vibrations – Mechanical Impedance of the human hand's glabrous skin". *Department of Environmental Medicine. University of Umea. S-901 87 Umea, Sweden. J. Biomechanics*, Vol. 17, No. 2., pp. 137-144, 1984.

[3] Ryan E. Schoonmaker, Caroline G.L. Cao, Member, IEEE. "Vibrotactile force feedback system for minimally invasive surgical procedure" *IEEE International conference on Systems, Man and Cybernetics*, Vol. 3, pp. 2464-2469, 2006.

[4] Hannes Hoppner, Dominic Lakatos, Holger Urbanek, Claudio Castellini and Patrick van der Smagt. "The Grasp Perturbator: Calibrating human grasp stiffness during a graded force task"., *IEEE International Conference on Robotics and Automation*, pp. 3312-3316, 2011.

[5] Alejandro Villasenor-Herrera, Sophie J. De Serres, Ross Wagner, Rober E. Kearney, Fellow, IEEE, 2008. "Exploring the Human Grip Force System: A preliminary Study". *Department of Biomedical Engineering, McGill University, Montreal, QC H3A, Canada., Annual International Conference of the IEEE, Engineering in Medicine and Biology Societey*, pp. 5362-5365, 2008.

[6] Gregorij Kurillo and Tadej Bajd, 2003. "Analysis of Human Grasping Using Robotic Force Sensor". *University of Ljubljana, Faculty of Electrical Engineering. IEEE International Conference on Industrial Technology*, Vol. 2, pp. 724-728, 2003.

[7] Hossein Mousavi Hondori, Ang Wei Tech, "Smart Mug to Measure Hand's Geometrical Mechanical Impedance". *Engineering in Medicine and Biology Society, International Conference of the IEEE*, pp. 4053-4056, 2011.

[8] J.L. Sancho-Bru, A. Perez-Gonzalez, M. Vergara-Monedero, D. Giurintano, 2001. "A 3-D dynamic model of human finger for studying free movements". *Departament de Tecnologia, Universitat Jaume I., Journal of Biomechanics*, Vol. 34, Issue 11, pp. 1491-1500, 2001.

[9] William J. Palm III, 2007. " Mechanical Vibration". *University of Rhode Island. John Wilwy & Sons, Inc.*

[10] Machine Perception Laboratory, Tutorials, Javier R. Movellan, 2010. " DC Motors". URL: http://mplab.ucsd.edu/wordpress/?page_id=75

[11] Precision Microdrives Limited. Registered in England and Wales, URL: http://www.precisionmicrodrives.com.

[12] Matlab product documentation, "DC Motors", URL: http://www.mathworks.com/help/toolbox/physmod/elec/ref/dcmotor.html.